Supplementary Tables

Supplementary Figures

Supplementary Notes

Supplementary Files

Files and datasets that are too large to include in this supplement are made available through http://noble.gs.washington.edu/proj/plasmo3d.

SuppFile1-mapping-and-filtering.xlsx This file summarizes the results of applying our mapping and filtering pipeline to the sequences from each Hi-C library generated in this work.

SuppFile2-contacts-at-0.1-FDR.xlsx This file lists, for each stage (ring, trophozoite, schizont), the set of contacts at 10 kb that were assigned a q-value < 0.1 (Methods). Rows are sorted from lowest to highest q-value and are colored using two other q-value thresholds (0.05 and 0.01).

SuppFile3-Var,Rif,Stevor,MC(VRSM)-clusters.xlsx This file contains the chromosomal coordinates of all *var*, *rifin*, *stevor*, and *Pfmc-2tm* (VRSM) genes, as well as the boundaries of subtelomeric and internal VRSM gene clusters.

SuppFile4-dynamic-model-all-chromosomes.mov This movie shows the dynamic changes in the architecture of all chromosomes during the *Plasmodium* erythrocytic cycle inferred by a linear interpolation of bead positions from one stage to the next by aligning the structures of adjacent stages. The movie starts and ends at the ring stage (ring–trophozoite–schizont–ring). Each chromosome is represented by a different color, and purple regions mark VRSM gene clusters. Telomeres are indicated by white spheres.

SuppFile{5–18}-dynamic-model-chr{1–14}.mov These movies are the same as the previous movie, but each focuses on a single chromosome.

Supplementary Tables

Supplementary Table 1: **Quality measures for Hi-C data.**

P. falciparum libraries are presented in this work and *S. cerevisiae* libraries from Duan et al. [1] are listed here for comparison. Rows marked with bold are control libraries that were generated without the cross-linking step of the Hi-C protocol. Interchromosomal contact probability (*ICP* [2]) and percent of long-range contacts (*PLRC*) values are computed as described in Methods.

Organism	*Library*	*ICP*	*PLRC*
P. falciparum	Ring	1.13	9.04%
	Trophozoite	0.66	7.64%
	Schizont	0.74	22.04%
	Trophozoite (not cross-linked)	**7.82**	**3.05%**
S. cerevisiae [1]	HindIII-MspI	1.92	8.99%
	HindIII-MseI	2.31	12.08%
	EcoRI-MspI	1.71	3.99%
	EcoRI-MseI	1.86	4.19%
	HindIII-MspI (not cross-linked)	**4.26**	**3.39%**

Supplementary Table 2: **GSEA results for genes involved in stage-specific contacts.**

For each stage, GSEA is applied to the set of genes that participate in contacts that are specific to that stage (Methods). For the *Type* column CC denotes "Cellular Component", MF denotes "Molecular Function" and BP denotes "Biological Process". Enrichments with q-value < 0.1 are shown.

Stage	*GO term*	*Description*	*Type*	*q-value*
Ring	GO:0020033	antigenic variation	BP	0.099
Trophozoite	GO:0020002	host cell plasma membrane	CC	0.004
	GO:0020030	infected host cell surface knob	CC	0.008
	GO:0016021	integral to membrane	CC	0.015
	GO:0004872	receptor activity	MF	0.007
	GO:0050839	cell adhesion molecule binding	MF	0.020
	GO:0020033	antigenic variation	BP	0.010
	GO:0009405	pathogenesis	BP	0.010
	GO:0020013	modulation by symbiont of host erythrocyte aggregation	BP	0.012
	GO:0020035	cytoadherence to microvasculature	BP	0.016
	GO:0016337	cell-cell adhesion	BP	0.022

Supplementary Table 3: **Assessing sensitivity of the 3D inference to different parameter settings.**

RMSD and distance difference values in nanometers (nm) between structures inferred from an unconstrained MDS with five different β values ranging from 0.4 to 0.6.

Stage	*RMSD* Mean (Standard deviation)	*Distance difference* Mean (Standard deviation)
Ring	10.39 (4.24)	5.75 (2.68)
Trophozoite	17.76 (6.57)	10.62 (4.65)
Schizont	12.90 (5.71)	8.10 (4.08)

Supplementary Table 4: **Assessing sensitivity of the 3D inference to spatial constraints.**

RMSD and distance difference values in nanometers (nm) between a structure inferred using constrained MDS and a structure from the corresponding unconstrained MDS.

Stage	*RMSD*	*Distance difference*
Ring	8.05	0.01
Trophozoite	61.99	0.83
Schizont	7.86	0.01

Supplementary Table 5: **Colocalization test for 21 gene/locus sets.**

We applied a previously described statistical test [3] to assess whether the loci in each set colocalize more than expected by chance (only interchromosomal pairs are considered). This test involves calculation of a colocalization statistic, which requires labeling of each locus pair as "close" or "far". We used varying distance thresholds (10%, 20% and 40% of the nuclear diameter) to deem a locus pair "close" and labeled all remaining pairs in the set as "far". We generated 3000 random locus sets to compute a p-value for each test. We corrected the p-values for multiple hypothesis testing using the Benjamini-Hochberg procedure [4] to compute the associated q-value. Grey color indicates a q-value < 0.05. Centromere coordinates were extracted from Hoeijmakers et al. [5]. Telomeres were defined as 20 kb regions at each end of each chromosome. The sets of internal and subtelomeric VRSM genes were tested all together as well as separately. The rDNA set consists of five units of 18S-5.8S-28S rDNA genes and one tandem of three 5S rDNA genes [6]. Clusters 1–15 correspond to expression clusters described in Le Roch et al. [7].

Gene set	*Ring*			*Trophozoite*			*Schizont*		
	10%	**20**%	**40**%	**10**%	**20**%	**40**%	**10**%	**20**%	**40**%
Centromeres	0.003	0.000	0.000	0.000	0.000	0.000	0.000	0.000	0.000
Telomeres	0.000	0.000	0.000	0.000	0.000	0.000	0.000	0.000	0.000
VRSM (all)	0.000	0.000	0.000	0.000	0.000	0.000	0.000	0.000	0.000
VRSM (internal)	0.388	0.215	0.070	0.152	0.023	0.079	0.246	0.077	0.025
VRSM (sub-telomeric)	0.000	0.000	0.000	0.000	0.000	0.000	0.000	0.000	0.000
rDNA genes	1.000	0.277	0.463	0.124	0.037	0.060	1.000	1.000	0.442
Cluster 1	0.103	0.011	0.115	0.018	0.133	0.133	0.135	0.007	0.013
Cluster 2	0.449	0.069	0.014	0.219	0.054	0.015	0.947	0.809	0.117
Cluster 3	0.215	0.014	0.075	0.437	0.002	0.001	0.758	0.809	0.033
Cluster 4	0.106	0.000	0.000	0.002	0.000	0.000	0.701	0.089	0.000
Cluster 5	0.449	0.701	0.291	0.779	0.045	0.002	0.508	0.528	0.682
Cluster 6	0.849	0.228	0.000	0.029	0.000	0.000	0.396	0.441	0.026
Cluster 7	0.291	0.000	0.000	0.596	0.001	0.074	0.704	0.523	0.011
Cluster 8	0.047	0.054	0.016	0.015	0.006	0.033	0.208	0.117	0.592
Cluster 9	0.508	0.063	0.014	0.040	0.001	0.002	0.468	0.809	0.117
Cluster 10	0.048	0.043	0.007	0.000	0.000	0.000	0.355	0.208	0.007
Cluster 11	0.198	0.019	0.063	0.411	0.000	0.000	0.601	0.446	0.013
Cluster 12	0.028	0.010	0.000	0.006	0.000	0.000	0.523	0.007	0.000
Cluster 13	0.091	0.021	0.075	0.033	0.003	0.000	0.711	0.028	0.001
Cluster 14	0.155	0.082	0.046	0.688	0.000	0.000	0.751	0.039	0.000
Cluster 15	0.046	0.014	0.103	0.016	0.058	0.002	0.758	0.809	0.011

Supplementary Table 6: **Sequences of primers used for the generation of FISH probes.**

Chr.	*Annotation*	*Locus (kb)*	*Forward primer*	*Reverse primer*
7	VRSM	550 - 560	5′-GATGGTAGAAGATAATAGGG -3′	5′-GACAAGTATAAGAACCAACC-3′
8	VRSM	40 - 50	5′-CGAAAGATAGTAGTGATGGT-3′	5′-CACTTATGCATTTCCATCCA-3′
7	Non-VRSM	810 - 820	5′-GCTTCCTTAATTGGACATTC-3′	5′-GAATTCGTTGGAGATTCTGT-3′
11	Non-VRSM	820 - 830	5′-CACTGAACAAGTAGTGTAATCA-3′	5′-GTTTCATCTTCAGAAGTAAGAG-3′
2	Non-VRSM	440 - 450	5′-GTTCCTACAGGTTTAGATCT-3′	5′-CATGAGGACATATTCACTTG-3′
4	Non-VRSM	1,160 - 1,170	5′-AAGTACAGGTGTAGGTAAAG-3′	5′-CGTAGCTTTAACCTGTTGTA-3′

Supplementary Table 7: **Gradient values of the log-linear fits that best capture the scaling of contact probability with genomic distance for each chromosome.**

Gradient (α) values for each chromosome at each stage calculated by fitting a power-law curve of the form $P(s) \sim s^{\alpha}$ to the intrachromosomal contact probability $P(s)$ as a function of genomic distance s. The reported α values are computed using raw contact maps at a single restriction enzyme fragment resolution for a genomic distance range of 20–250 kb.

Chromosome	*Ring*	*Trophozoite*	*Schizont*
1	-1.02	-1.18	-1.04
2	-0.99	-1.22	-1.01
3	-0.99	-1.20	-0.98
4	-0.97	-1.13	-0.99
5	-0.97	-1.14	-0.96
6	-1.01	-1.19	-1.00
7	-1.02	-1.27	-1.01
8	-1.00	-1.19	-0.98
9	-0.99	-1.11	-0.94
10	-0.97	-1.14	-0.96
11	-0.97	-1.11	-0.94
12	-0.99	-1.14	-0.97
13	-0.97	-1.07	-0.93
14	-0.98	-1.09	-0.93

Supplementary Table 8: **GSEA results for the ring stage on the first component of the kCCA.**

GSEA is applied to the ranked list of genes per projection on the kCCA component. For the *Enrichment* column, t denotes enrichment near the telomeres, and n-t denotes enrichment in non-telomeric regions. For the *Type* column CC denotes "Cellular Component", MF denotes "Molecular Function" and BP denotes "Biological Process". Enrichments with q-value < 0.1 are shown.

GO term	*Description*	*Type*	*Enrichment*	*q-value*
GO:0020002	host cell plasma membrane	CC	t	0.000
GO:0020030	infected host cell surface knob	CC	t	0.000
GO:0020036	Maurer's cleft	CC	t	0.000
GO:0005840	ribosome	CC	n-t	0.000
GO:0005622	intracellular	CC	n-t	0.000
GO:0022627	cytosolic small ribosomal subunit	CC	n-t	0.000
GO:0022625	cytosolic large ribosomal subunit	CC	n-t	0.000
GO:0015935	small ribosomal subunit	CC	n-t	0.000
GO:0005783	endoplasmic reticulum	CC	n-t	0.000
GO:0015934	large ribosomal subunit	CC	n-t	0.000
GO:0005789	endoplasmic reticulum membrane	CC	n-t	0.000
GO:0005839	proteasome core complex	CC	n-t	0.006
GO:0005794	Golgi apparatus	CC	n-t	0.008
GO:0005829	cytosol	CC	n-t	0.008
GO:0005739	mitochondrion	CC	n-t	0.018
GO:0016021	integral to membrane	CC	t	0.034
GO:0005694	chromosome	CC	n-t	0.064
GO:0004872	receptor activity	MF	t	0.000
GO:0050839	cell adhesion molecule binding	MF	t	0.000
GO:0046789	host cell surface receptor binding	MF	t	0.000
GO:0003735	structural constituent of ribosome	MF	n-t	0.000
GO:0004175	endopeptidase activity	MF	n-t	0.010
GO:0003677	DNA binding	MF	n-t	0.011
GO:0005215	transporter activity	MF	n-t	0.034
GO:0004298	threonine-type endopeptidase activity	MF	n-t	0.035
GO:0003676	nucleic acid binding	MF	n-t	0.094
GO:0016881	acid-amino acid ligase activity	MF	n-t	0.094
GO:0020033	antigenic variation	BP	t	0.000
GO:0009405	pathogenesis	BP	t	0.000
GO:0020035	cytoadherence to microvasculature	BP	t	0.000
GO:0020013	modulation by symbiont of host erythrocyte aggregation	BP	t	0.000
GO:0016337	cell-cell adhesion	BP	t	0.000
GO:0006412	translation	BP	n-t	0.000
GO:0006886	intracellular protein transport	BP	n-t	0.000
GO:0006511	ubiquitin-dependent protein catabolic process	BP	n-t	0.001
GO:0045454	cell redox homeostasis	BP	n-t	0.019
GO:0007264	small GTPase mediated signal transduction	BP	n-t	0.025
GO:0006281	DNA repair	BP	n-t	0.025
GO:0006260	DNA replication	BP	n-t	0.025
GO:0016192	vesicle-mediated transport	BP	n-t	0.027
GO:0006414	translational elongation	BP	n-t	0.029
GO:0015031	protein transport	BP	n-t	0.029

Supplementary Table 9: **GSEA results for the trophozoite stage on the first component of the kCCA.**

GSEA is applied to the ranked list of genes per projection on the kCCA component. For the *Enrichment* column, t denotes enrichment near the telomeres, and n-t denotes enrichment in non-telomeric regions. For the *Type* column CC denotes "Cellular Component", MF denotes "Molecular Function" and BP denotes "Biological Process". Enrichments with q-value < 0.1 are shown.

GO term	*Description*	*Type*	*Enrichment*	*q-value*
GO:0005840	ribosome	CC	n-t	0.000
GO:0005622	intracellular	CC	n-t	0.000
GO:0022627	cytosolic small ribosomal subunit	CC	n-t	0.000
GO:0005789	endoplasmic reticulum membrane	CC	n-t	0.000
GO:0005783	endoplasmic reticulum	CC	n-t	0.000
GO:0022625	cytosolic large ribosomal subunit	CC	n-t	0.000
GO:0015935	small ribosomal subunit	CC	n-t	0.000
GO:0020002	host cell plasma membrane	CC	t	0.000
GO:0020030	infected host cell surface knob	CC	t	0.000
GO:0020036	Maurer's cleft	CC	t	0.000
GO:0016021	integral to membrane	CC	t	0.000
GO:0015934	large ribosomal subunit	CC	n-t	0.001
GO:0005794	Golgi apparatus	CC	n-t	0.005
GO:0005739	mitochondrion	CC	n-t	0.028
GO:0005839	proteasome core complex	CC	n-t	0.084
GO:0005829	cytosol	CC	n-t	0.087
GO:0003735	structural constituent of ribosome	MF	n-t	0.000
GO:0004872	receptor activity	MF	t	0.000
GO:0050839	cell adhesion molecule binding	MF	t	0.000
GO:0046789	host cell surface receptor binding	MF	t	0.000
GO:0005215	transporter activity	MF	n-t	0.003
GO:0003677	DNA binding	MF	n-t	0.059
GO:0005509	calcium ion binding	MF	n-t	0.088
GO:0020033	antigenic variation	BP	t	0.000
GO:0009405	pathogenesis	BP	t	0.000
GO:0016337	cell-cell adhesion	BP	t	0.000
GO:0020035	cytoadherence to microvasculature	BP	t	0.000
GO:0020013	modulation by symbiont of host erythrocyte aggregation	BP	t	0.000
GO:0006412	translation	BP	n-t	0.000
GO:0045454	cell redox homeostasis	BP	n-t	0.011
GO:0006886	intracellular protein transport	BP	n-t	0.012
GO:0006511	ubiquitin-dependent protein catabolic process	BP	n-t	0.099

Supplementary Table 10: **GSEA results for the schizont stage on the first component of the kCCA.**

GSEA is applied to the ranked list of genes per projection on the kCCA component. For the *Enrichment* column, t denotes enrichment near the telomeres, and n-t denotes enrichment in non-telomeric regions. For the *Type* column CC denotes "Cellular Component", MF denotes "Molecular Function" and BP denotes "Biological Process". Enrichments with q-value < 0.1 are shown.

GO term	*Description*	*Type*	*Enrichment*	*q-value*
GO:0020030	infected host cell surface knob	CC	t	0.000
GO:0005840	ribosome	CC	n-t	0.000
GO:0005622	intracellular	CC	n-t	0.000
GO:0022627	cytosolic small ribosomal subunit	CC	n-t	0.000
GO:0022625	cytosolic large ribosomal subunit	CC	n-t	0.000
GO:0005783	endoplasmic reticulum	CC	n-t	0.000
GO:0015935	small ribosomal subunit	CC	n-t	0.000
GO:0020036	Maurer's cleft	CC	t	0.000
GO:0020002	host cell plasma membrane	CC	t	0.000
GO:0015934	large ribosomal subunit	CC	n-t	0.001
GO:0005789	endoplasmic reticulum membrane	CC	n-t	0.001
GO:0005839	proteasome core complex	CC	n-t	0.002
GO:0016021	integral to membrane	CC	t	0.003
GO:0005794	Golgi apparatus	CC	n-t	0.008
GO:0005739	mitochondrion	CC	n-t	0.026
GO:0004872	receptor activity	MF	t	0.000
GO:0050839	cell adhesion molecule binding	MF	t	0.000
GO:0046789	host cell surface receptor binding	MF	t	0.000
GO:0003735	structural constituent of ribosome	MF	n-t	0.000
GO:0004175	endopeptidase activity	MF	n-t	0.008
GO:0005215	transporter activity	MF	n-t	0.011
GO:0003677	DNA binding	MF	n-t	0.013
GO:0004298	threonine-type endopeptidase activity	MF	n-t	0.015
GO:0020033	antigenic variation	BP	t	0.000
GO:0009405	pathogenesis	BP	t	0.000
GO:0020013	modulation by symbiont of host erythrocyte aggregation	BP	t	0.000
GO:0020035	cytoadherence to microvasculature	BP	t	0.000
GO:0016337	cell-cell adhesion	BP	t	0.000
GO:0006412	translation	BP	n-t	0.000
GO:0006511	ubiquitin-dependent protein catabolic process	BP	n-t	0.002
GO:0006886	intracellular protein transport	BP	n-t	0.003
GO:0045454	cell redox homeostasis	BP	n-t	0.016
GO:0007264	small GTPase mediated signal transduction	BP	n-t	0.017
GO:0006260	DNA replication	BP	n-t	0.028
GO:0015031	protein transport	BP	n-t	0.043
GO:0006281	DNA repair	BP	n-t	0.091
GO:0016192	vesicle-mediated transport	BP	n-t	0.091

Supplementary Table 11: **kCCA enrichment of 15 expression clusters.**

GSEA is applied to the ranked list of genes per projection on the first and second kCCA components (*Comp*), relative to 15 expression clusters defined by Le Roch et al. [7] (*Cluster*). For the enrichment column (*Enr.*), *t* refers to an enrichment in telomeric regions, *n-t* to an enrichment in non-telomeric regions, *c* to enrichment in the centromeric regions, and *n-c* to enrichment in non-centromeric regions. Enrichments with q-values < 0.05 are shaded grey.

Comp	*Cluster*	*Ring*		*Trophozoite*		*Schizont*	
		q-value	*Enr.*	*q-value*	*Enr.*	*q-value*	*Enr.*
1	1	0.000	n-t	0.000	n-t	0.000	n-t
	2	0.358	n-t	0.730	n-t	0.667	n-t
	3	0.000	t	0.000	t	0.000	t
	4	0.000	n-t	0.000	n-t	0.000	n-t
	5	0.482	t	0.216	t	0.997	t
	6	0.000	t	0.003	t	0.003	t
	7	0.036	t	0.818	n-t	1.000	n-t
	8	0.759	n-t	0.897	n-t	0.819	n-t
	9	0.000	t	0.000	t	0.000	t
	10	0.000	t	0.000	t	0.000	t
	11	0.011	t	0.000	t	0.000	t
	12	0.000	t	0.000	t	0.000	t
	13	0.000	t	0.000	t	0.000	t
	14	0.000	t	0.000	t	0.000	t
	15	0.230	n-t	0.703	n-t	0.924	n-t
2	1	0.000	n-c	0.000	n-c	0.000	n-c
	2	0.006	n-c	0.002	n-c	0.005	n-c
	3	0.000	c	0.000	c	0.000	c
	4	0.000	c	0.000	c	0.000	c
	5	0.686	c	1.000	c	0.980	n-c
	6	0.838	c	1.000	c	0.999	c
	7	0.000	c	0.000	c	0.000	c
	8	0.956	n-c	1.000	c	1.000	n-c
	9	0.004	c	0.000	c	0.000	c
	10	0.071	n-c	0.996	c	1.000	n-c
	11	0.000	n-c	0.000	n-c	0.000	n-c
	12	0.000	n-c	0.000	n-c	0.000	n-c
	13	0.000	n-c	0.000	n-c	0.002	n-c
	14	0.000	n-c	0.000	n-c	0.000	n-c
	15	0.000	n-c	0.000	n-c	0.000	n-c

Supplementary Table 12: **GSEA results for the second component of the kCCA.**

GSEA is applied to the ranked list of genes per projection on the kCCA component. For the *Enrichment* column, *c* denotes enrichment near the centromeres, *n-c* denotes enrichment in non centromeric regions. For the *Type* column CC denotes "Cellular Component", MF denotes "Molecular Function" and BP denotes "Biological Process". Enrichments with q-value < 0.1 are shown.

Stage	*GO term*	*Description*	*Type*	*Enrichment*	*q-value*
Ring	GO:0020008	rhoptry	CC	n-c	0.014
	GO:0016459	myosin complex	CC	n-c	0.020
	GO:0005839	proteasome core complex	CC	n-c	0.031
	GO:0008234	cysteine-type peptidase activity	MF	n-c	0.001
	GO:0004713	protein tyrosine kinase activity	MF	n-c	0.007
	GO:0003779	actin binding	MF	n-c	0.009
	GO:0004175	endopeptidase activity	MF	n-c	0.015
	GO:0004298	threonine-type endopeptidase activity	MF	n-c	0.018
	GO:0003774	motor activity	MF	n-c	0.035
	GO:0005516	calmodulin binding	MF	n-c	0.039
	GO:0016255	attachment of GPI anchor to protein	BP	n-c	0.066
Trophozoite	GO:0005839	proteasome core complex	CC	n-c	0.033
	GO:0020008	rhoptry	CC	n-c	0.058
	GO:0016459	myosin complex	CC	n-c	0.084
	GO:0008234	cysteine-type peptidase activity	MF	n-c	0.000
	GO:0004175	endopeptidase activity	MF	n-c	0.028
	GO:0004713	protein tyrosine kinase activity	MF	n-c	0.029
	GO:0004298	threonine-type endopeptidase activity	MF	n-c	0.029
	GO:0003779	actin binding	MF	n-c	0.048
	GO:0003774	motor activity	MF	n-c	0.090
	GO:0005516	calmodulin binding	MF	n-c	0.093
	GO:0016740	transferase activity	MF	n-c	0.099
	GO:0016255	attachment of GPI anchor to protein	BP	n-c	0.036
Schizont	GO:0005839	proteasome core complex	CC	n-c	0.026
	GO:0020008	rhoptry	CC	n-c	0.044
	GO:0016459	myosin complex	CC	n-c	0.083
	GO:0008234	cysteine-type peptidase activity	MF	n-c	0.000
	GO:0004175	endopeptidase activity	MF	n-c	0.013
	GO:0004298	threonine-type endopeptidase activity	MF	n-c	0.018
	GO:0004713	protein tyrosine kinase activity	MF	n-c	0.019
	GO:0003779	actin binding	MF	n-c	0.053

Supplementary Table 13: **Density score for varying values of β parameter at different stages.**

For each stage the β value that yields the minimal density score (shown in boldface) is used for three-dimensional modeling.

Stage	$\beta = 0.4$	$\beta = 0.45$	$\beta = 0.5$	$\beta = 0.55$	$\beta = 0.6$
Ring	0.109	0.077	**0.057**	0.063	0.110
Trophozoite	0.127	0.087	0.048	**0.044**	0.540
Schizont	0.051	**0.048**	0.128	0.313	0.591

Supplementary Figures

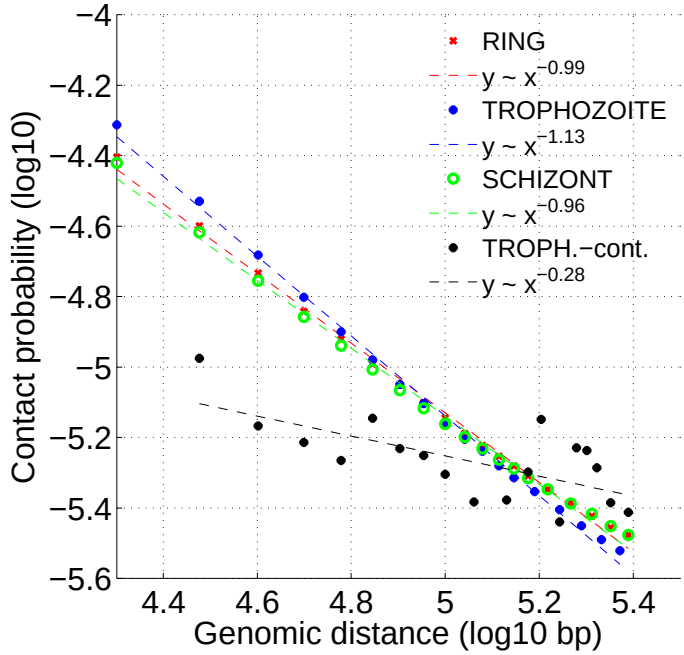

(a)

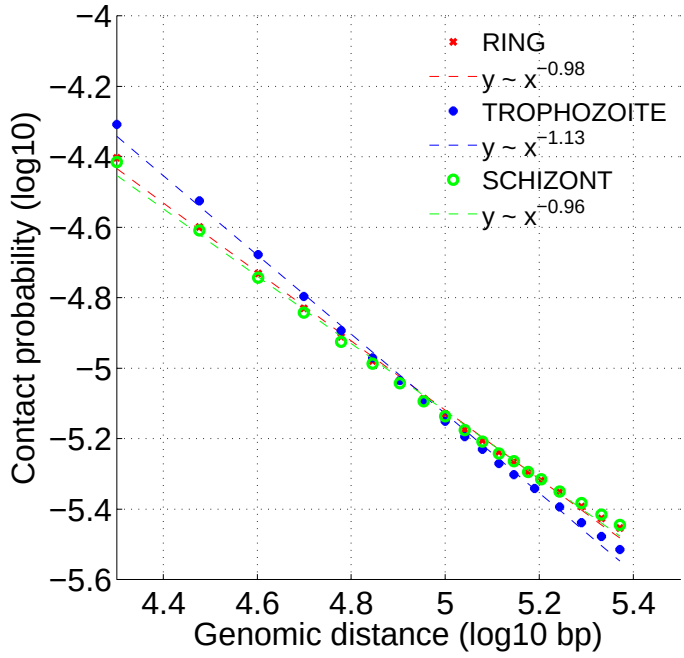

(b)

Supplementary Figure 1: **Power-law fits to 10 kb aggregated data.**
A power law of the form $P(s) \sim s^{\alpha}$ is fit to the intrachromosomal contact probability $P(s)$ as a function of genomic distance s for each stage (Methods). These log-linear fits are visualized by dashed lines and the corresponding gradient (α) values are reported in the legend for (a) raw and (b) normalized Hi-C contact maps at 10 kb resolution.

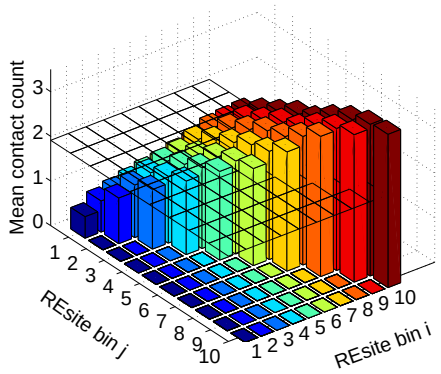

(a) Before normalization - No. of RE cut sites

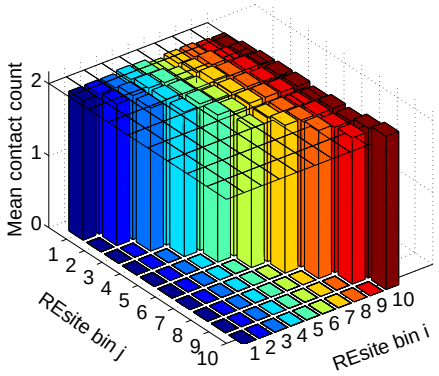

(b) After normalization - No. of RE cut sites

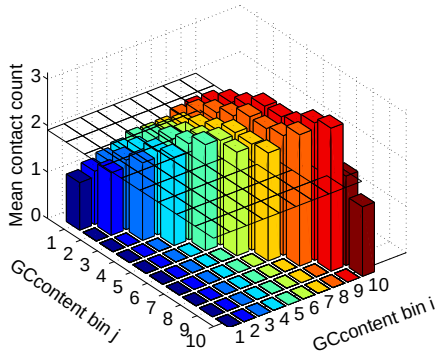

(c) Before normalization - Mappability

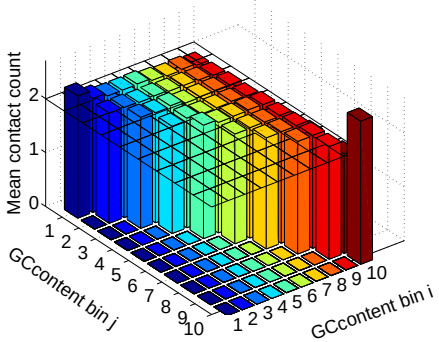

(d) After normalization - Mappability

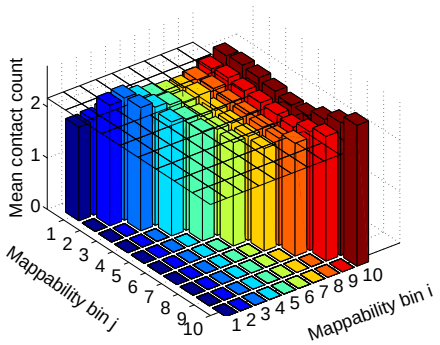

(e) Before normalization - GC content

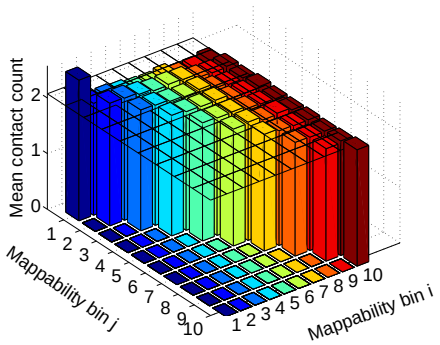

(f) After normalization - GC content

Supplementary Figure 2: **Biases in raw and corrected contact maps for ring stage.** For each non-overlapping 10 kb window in the genome we compute a genomic feature such as the number of restriction enzyme (RE) cut sites, the fraction of uniquely mappable bases and GC content. For each feature, we group all windows into 10 equal sized bins based on the feature value. Each possible locus pair belongs to one specific bin pair (2D bin) which is indexed by the two horizontal axes. For each 2D bin we compute the mean contact count using all locus pairs that fall into that bin. The black, horizontal grid plane corresponds to the overall mean. For perfectly unbiased data all vertical bars will be of equal height and equal to the overall mean. (a, c, e) and (b, d, f) plots show biases for each indicated feature before and after normalization, respectively. Plots for trophozoite and schizont stages are similar (data not shown).

Supplementary Figure 3: **Chromosome visualizations.**

In the following fourteen pages, each page of figures corresponds to one chromosome, with the three time points (ring, trophozoite, schizont) arranged in three columns. Within each column, the top panels show the 10kb resolution contact count matrix after normalization using ICE [8], the p-values assigned to contacts, and the pairwise Euclidean distances derived from the 3D model. Within each matrix, clusters of VSRM genes are indicated with yellow boxes, and centromere locations are indicated with blue dotted lines. The fourth panel in each column illustrates the eigenvalue analysis, with compartment boundaries aggregated over the three stages (Methods) indicated by black dotted lines. The bottom panel shows the chromosome's inferred configuration in 3D with light blue spheres indicating centomeres, white spheres indicating telomeres and green spheres indicating midpoints of VRSM gene clusters.

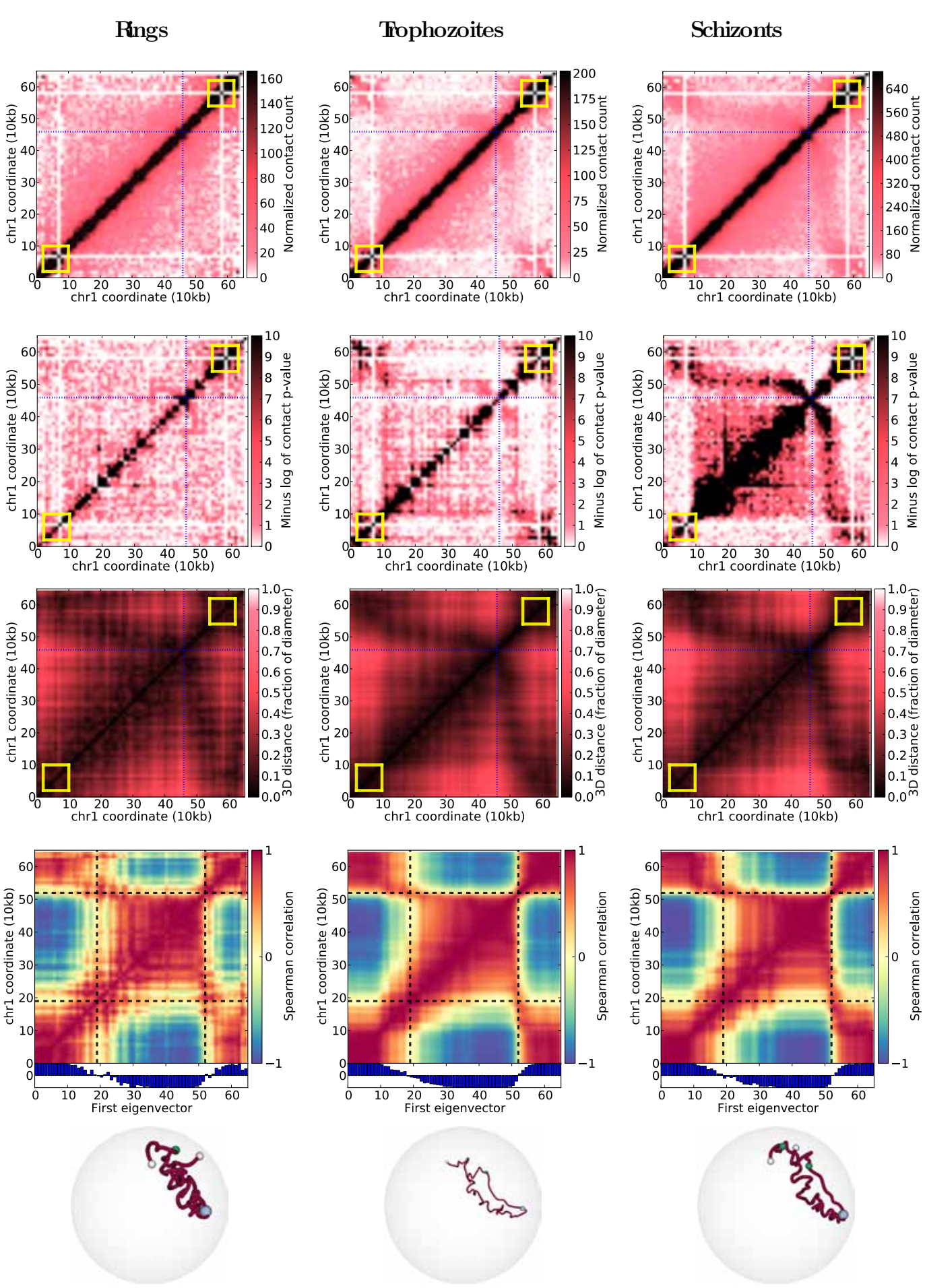

(a) Chromosome 1

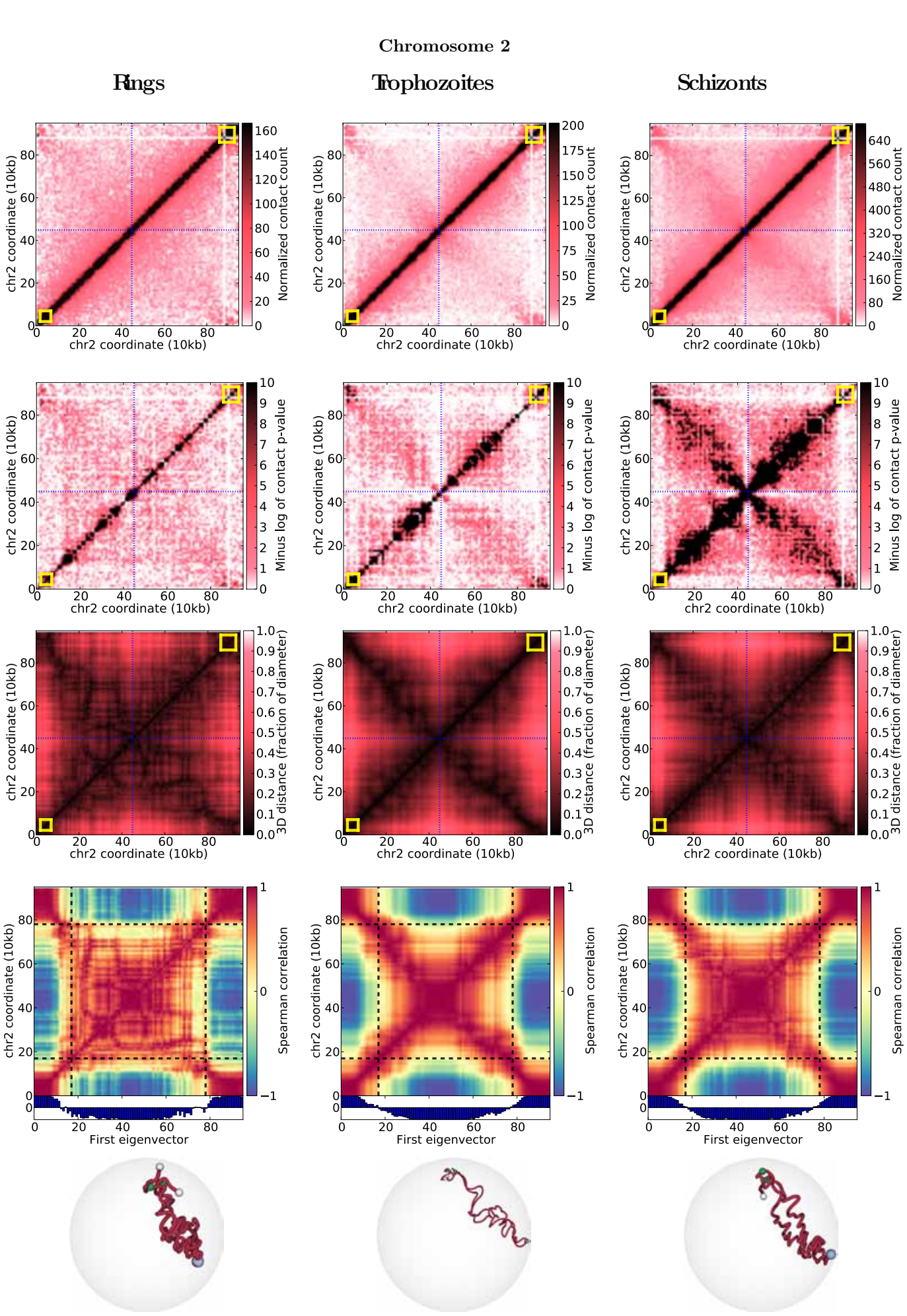

(b) Chromosome 2

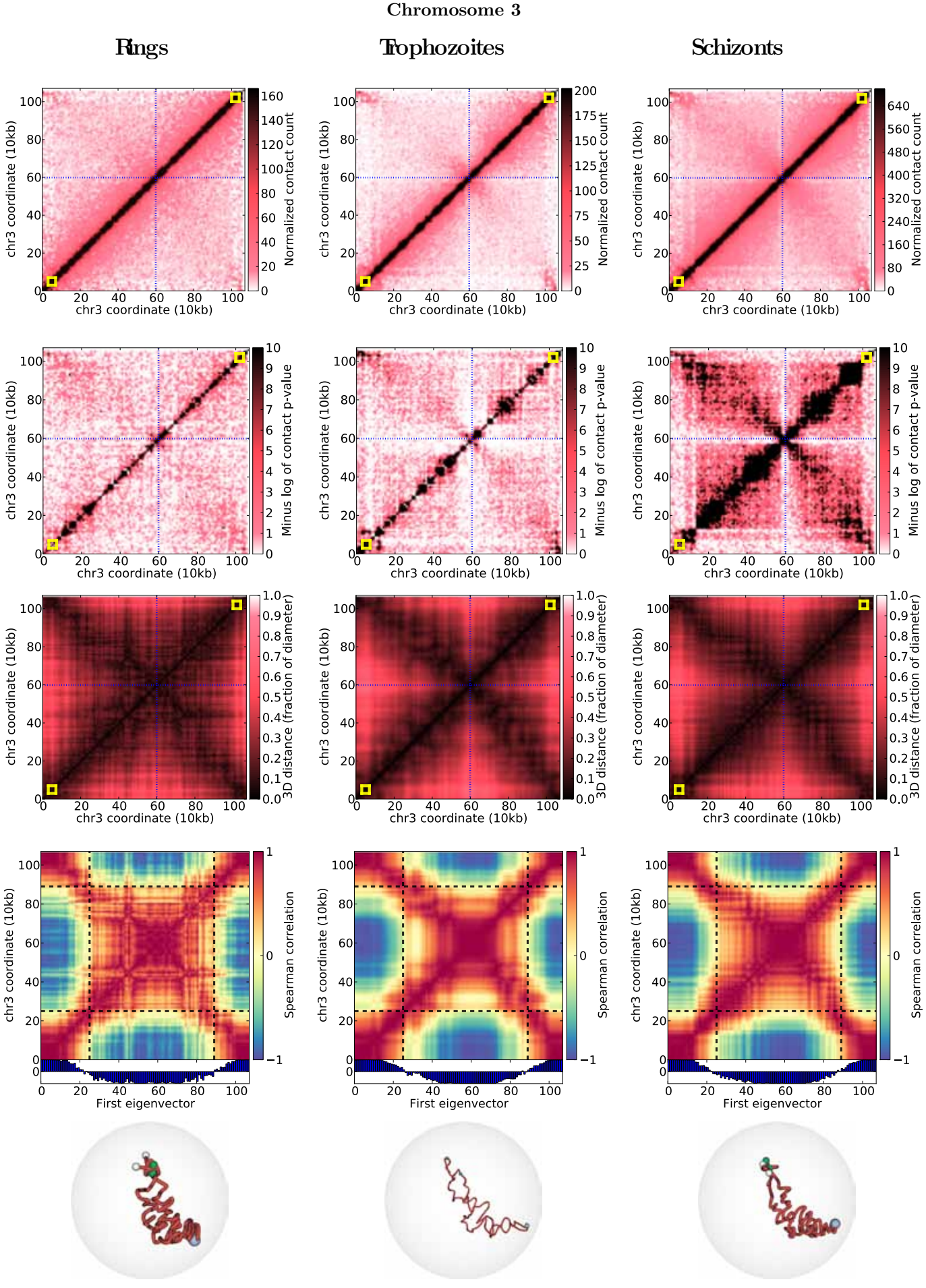

(c) Chromosome 3

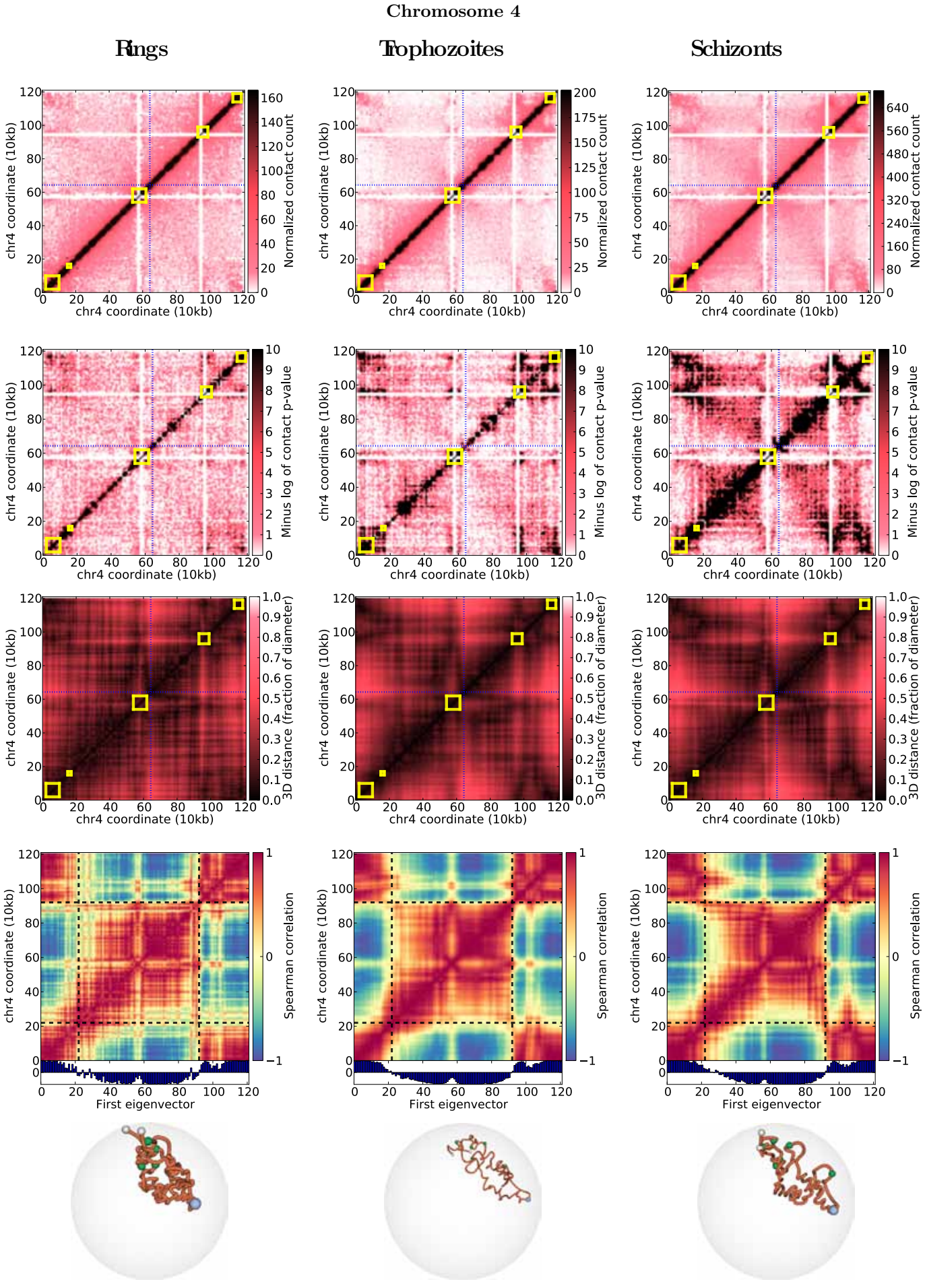

(d) Chromosome 4

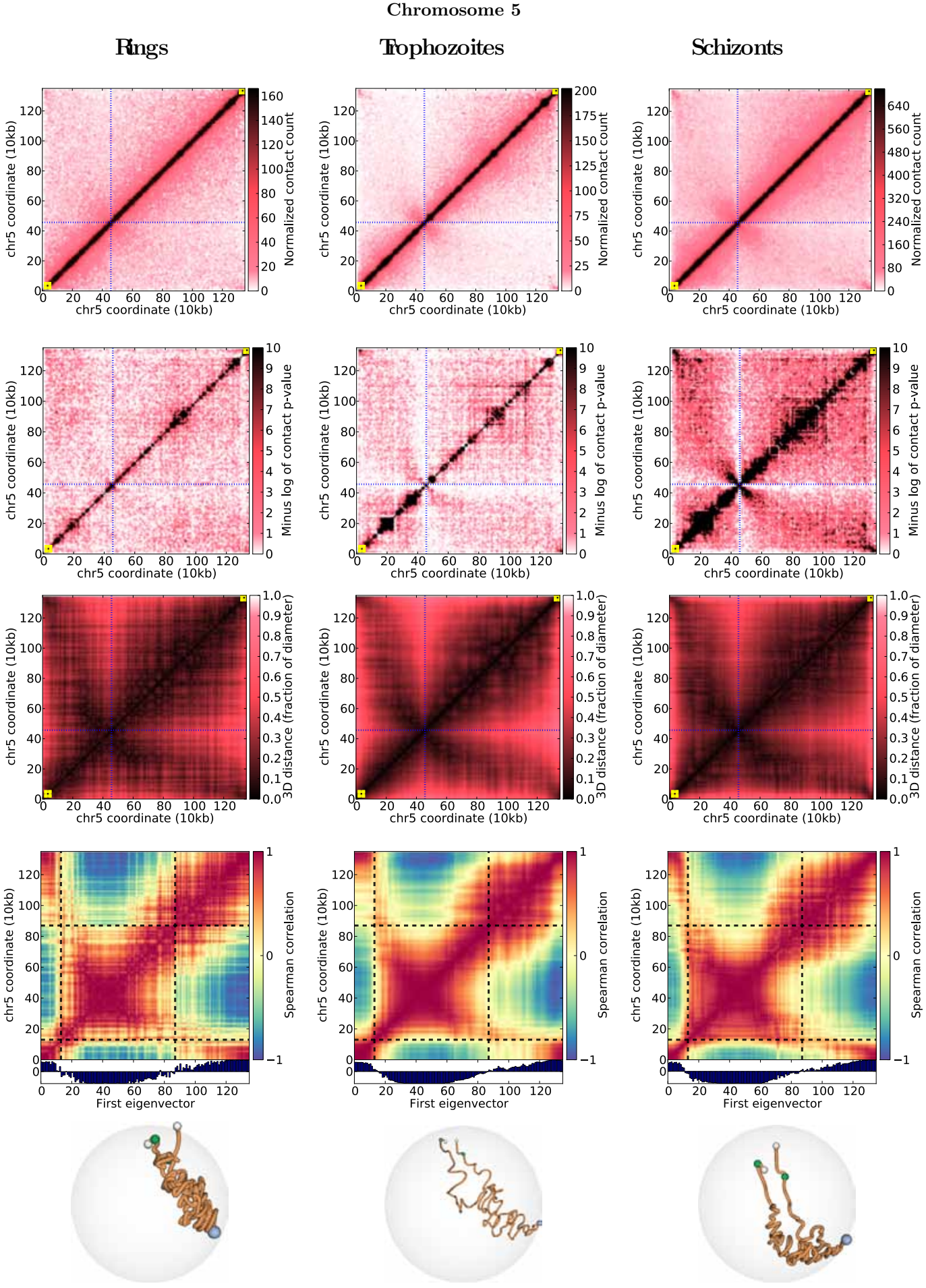

(e) Chromosome 5

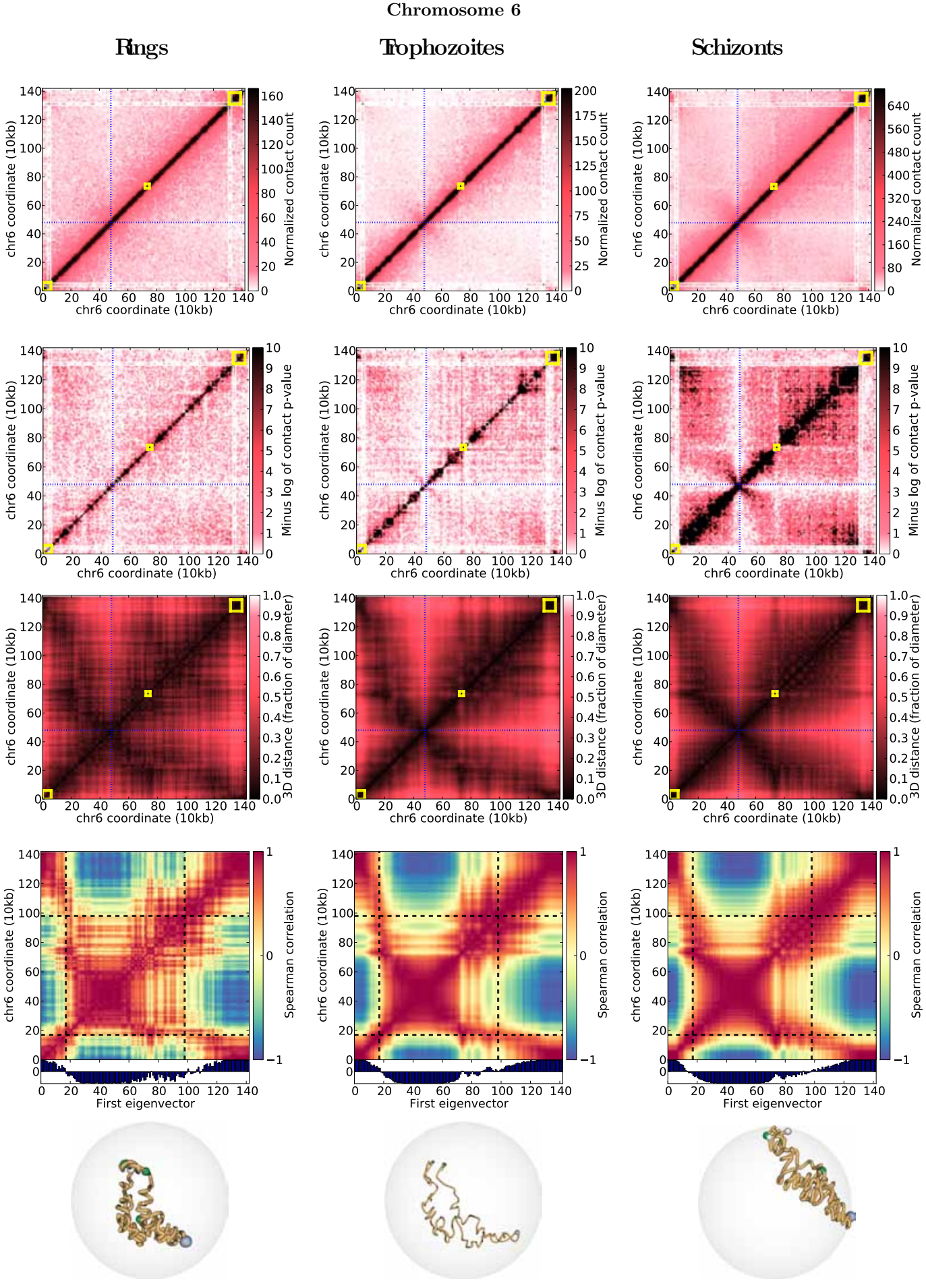

(f) Chromosome 6

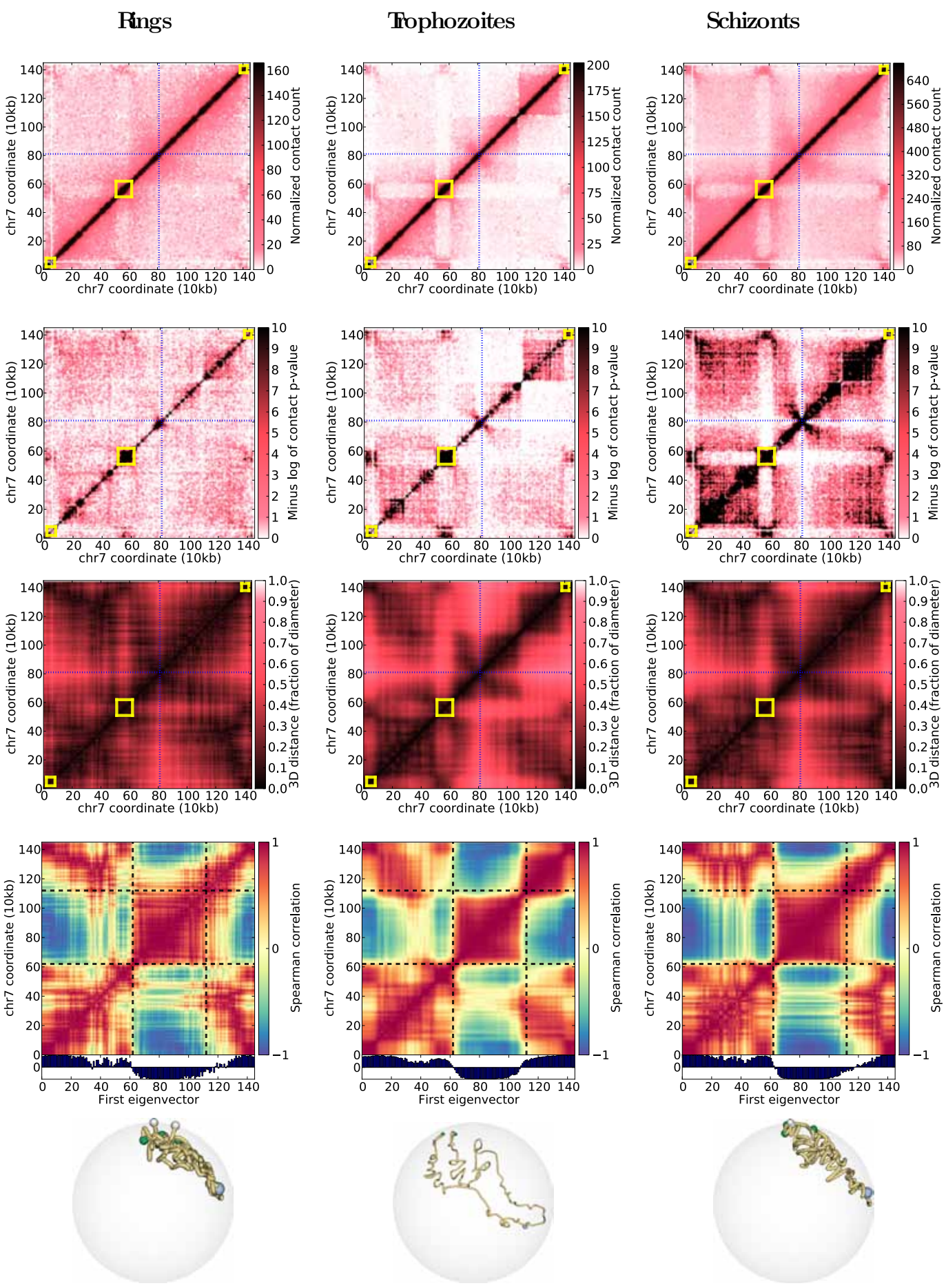

(g) Chromosome 7

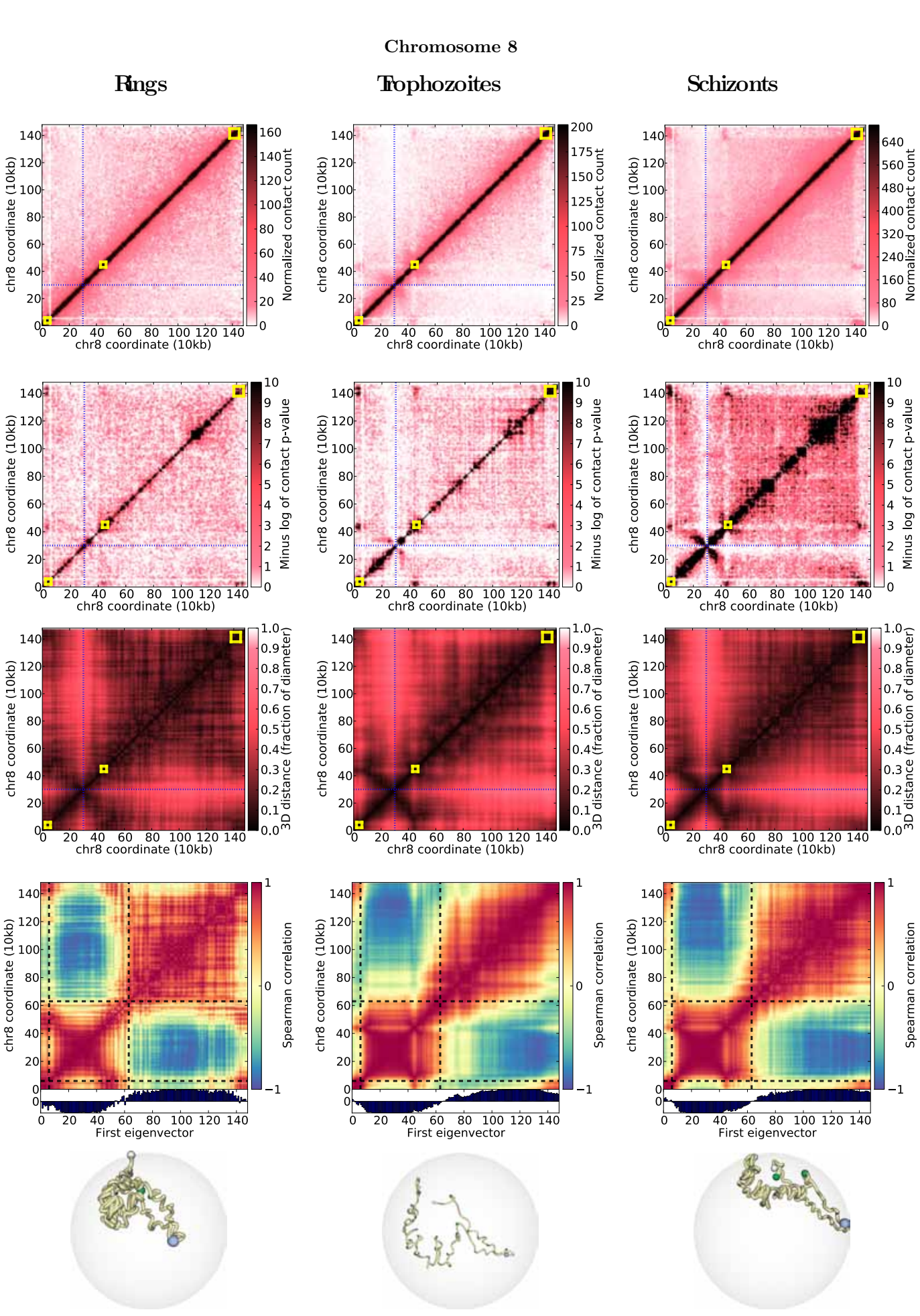

(h) Chromosome 8

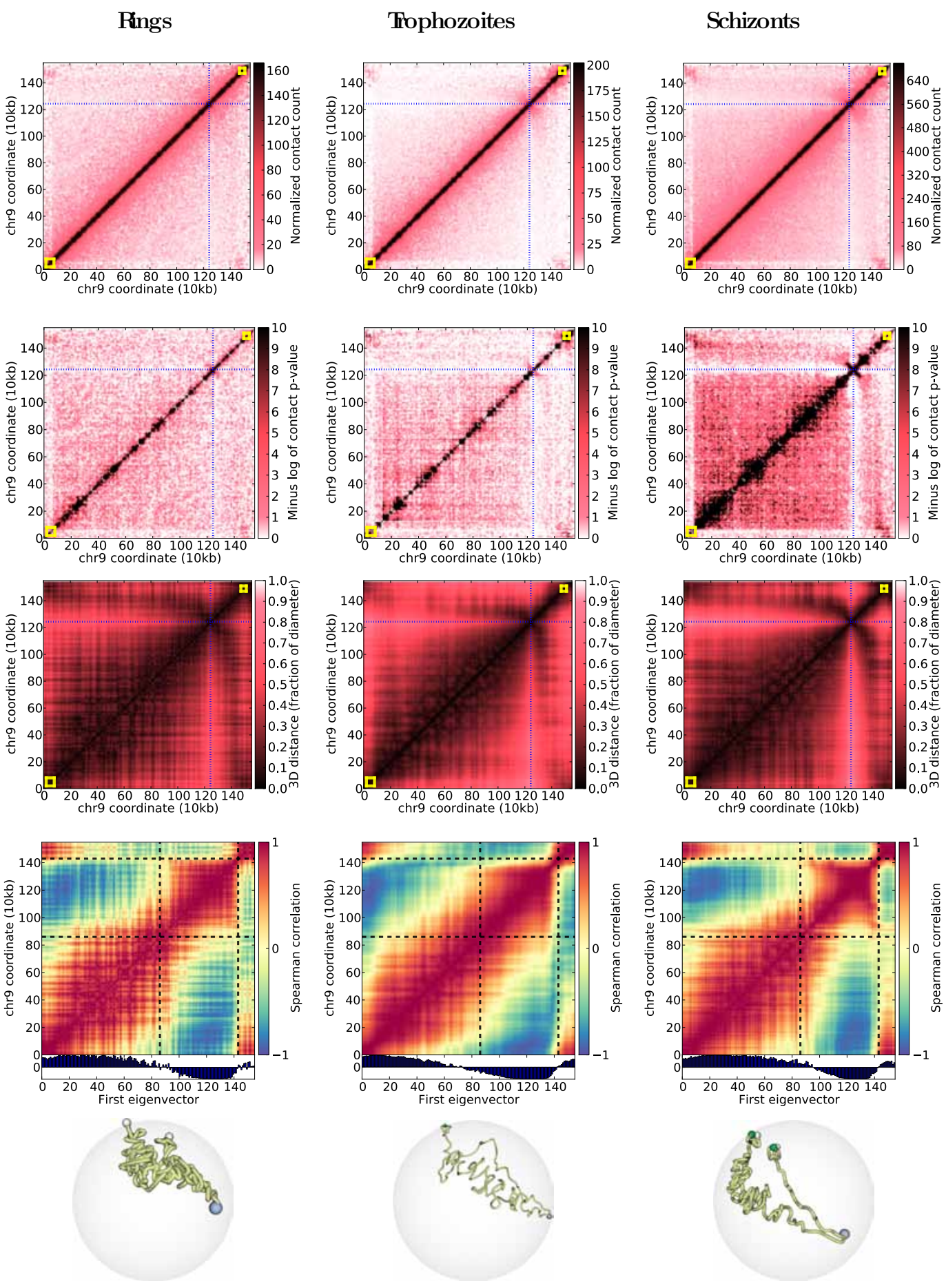

(i) Chromosome 9

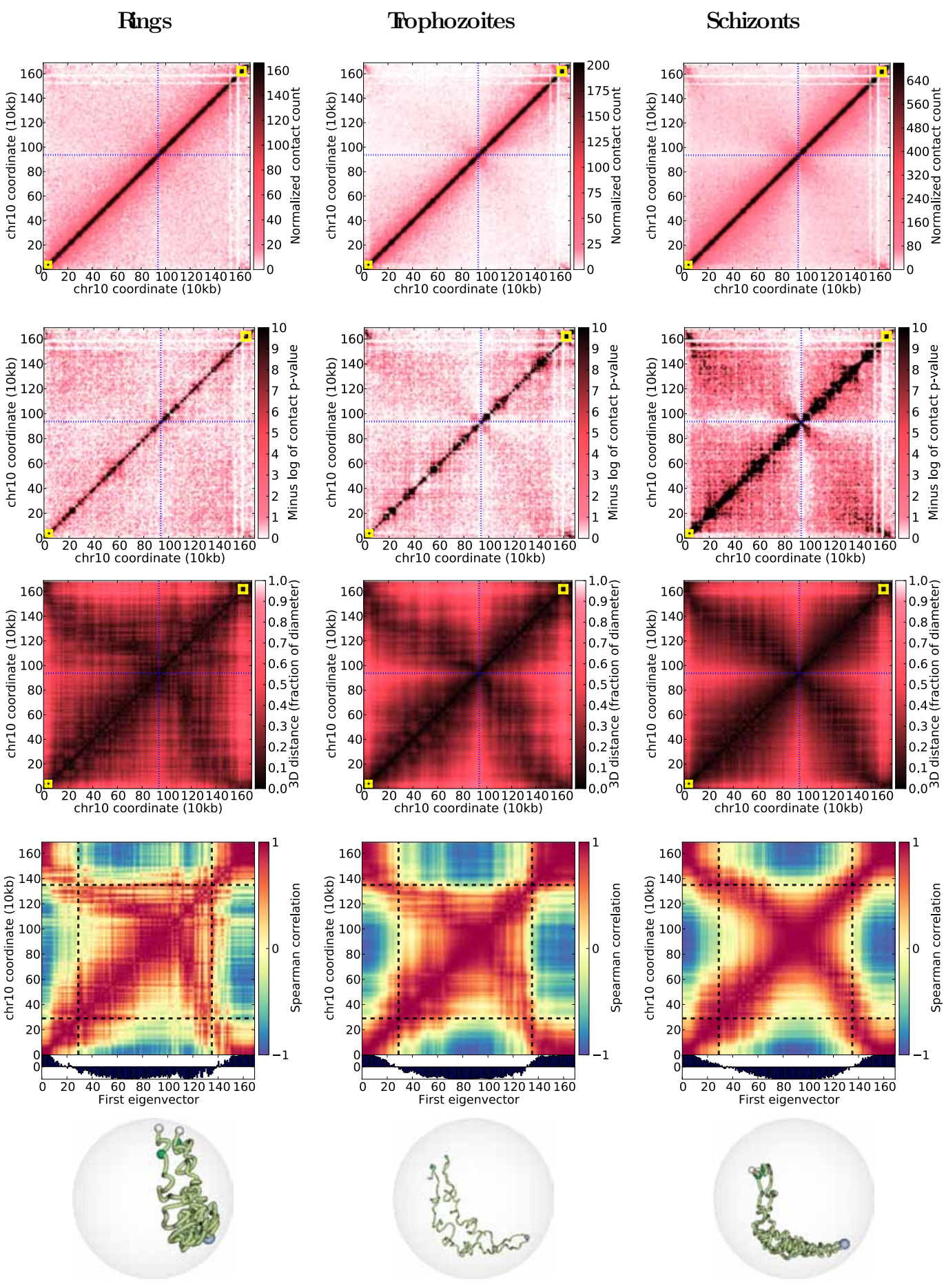

(j) Chromosome 10

Chromosome 11

Rings

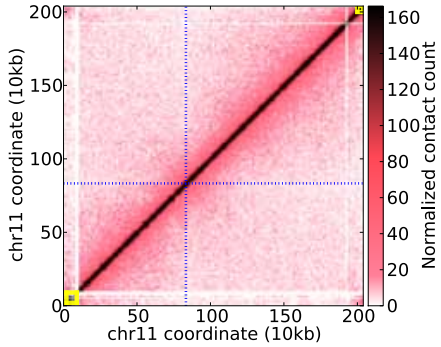

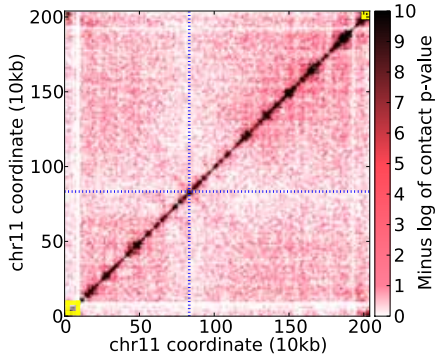

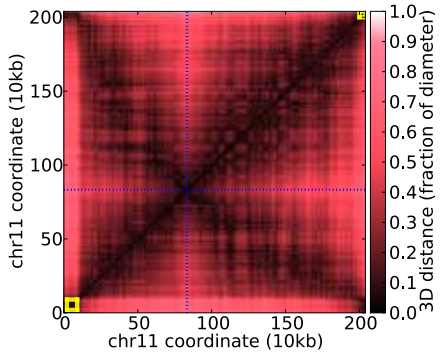

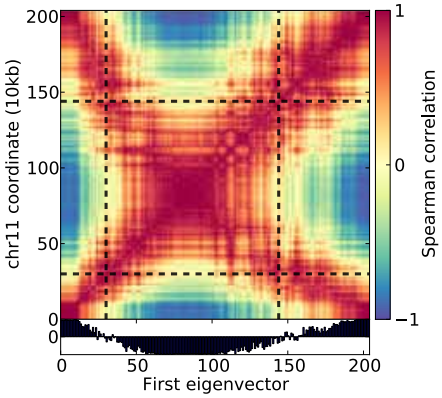

Trophozoites

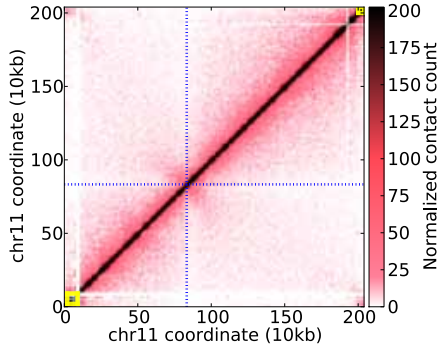

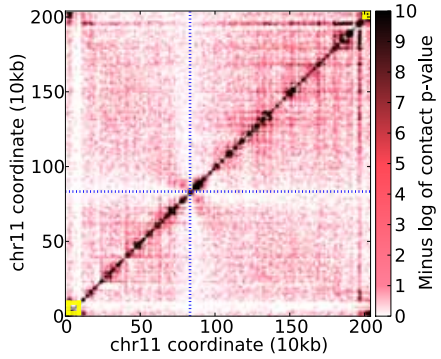

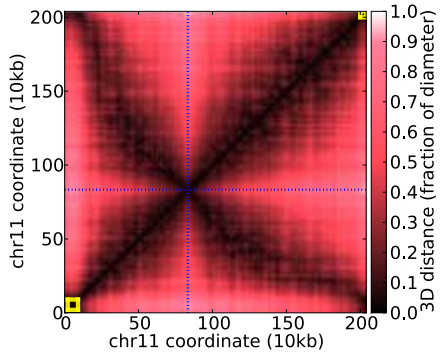

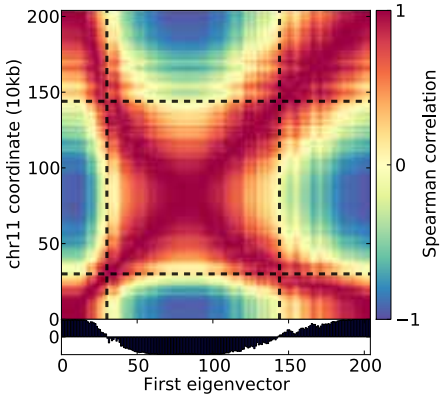

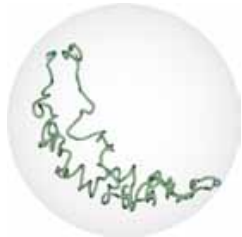

Schizonts

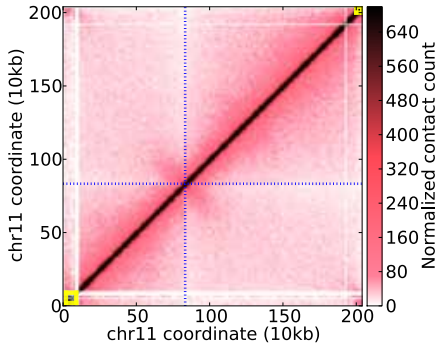

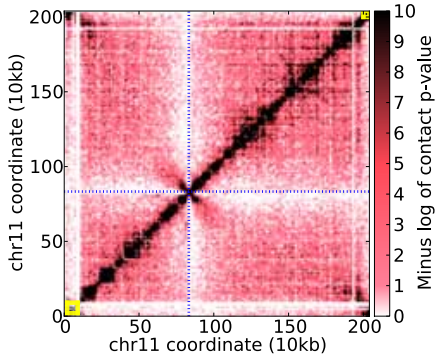

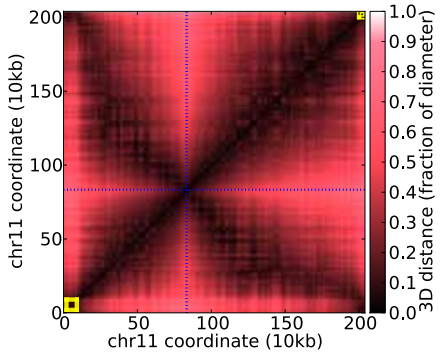

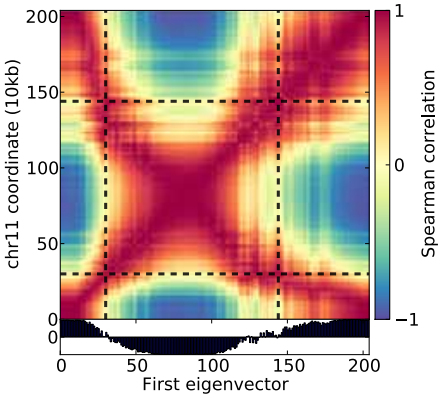

(k) Chromosome 11

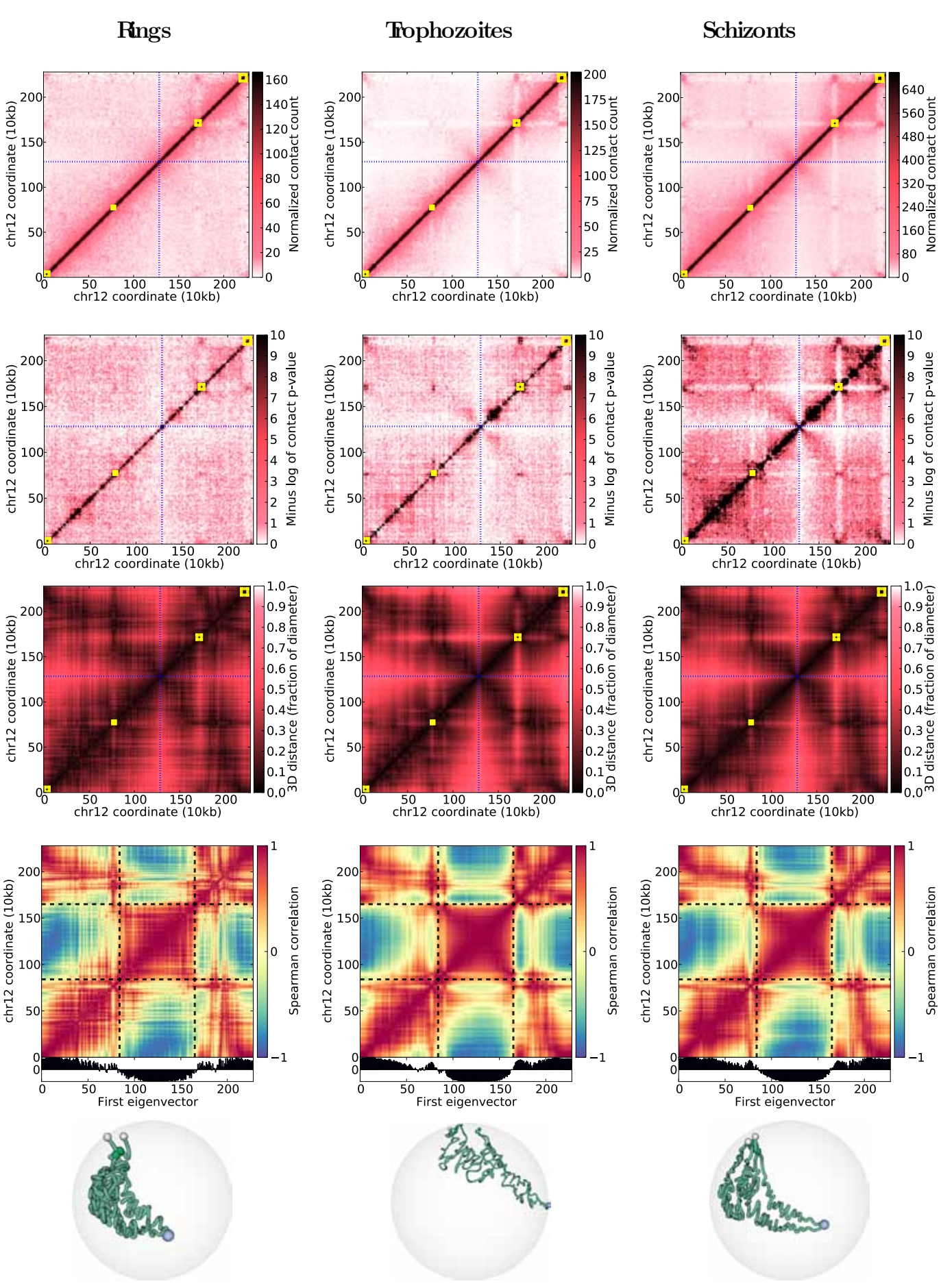

(l) Chromosome 12

Chromosome 13

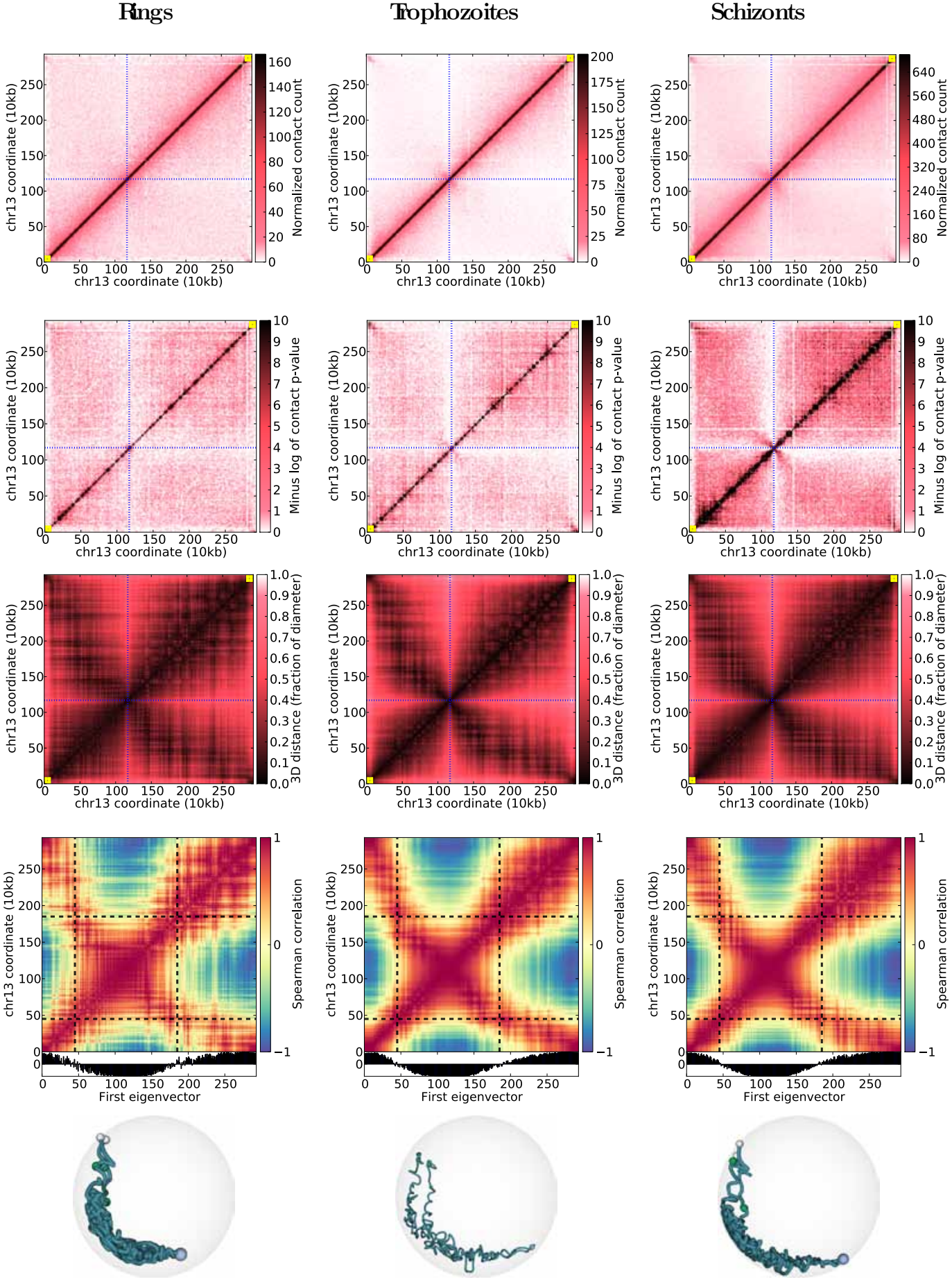

(m) Chromosome 13

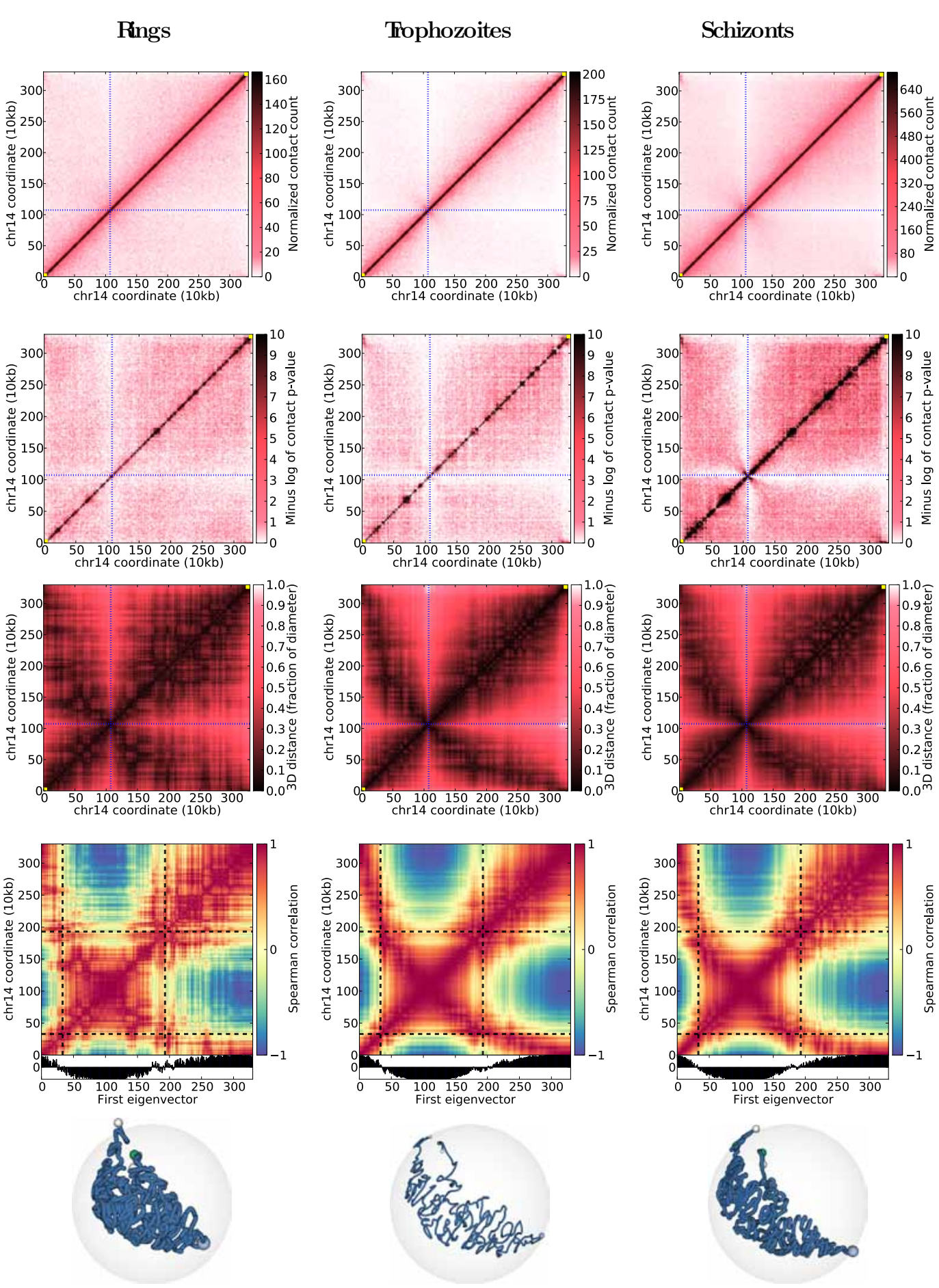

(n) Chromosome 14

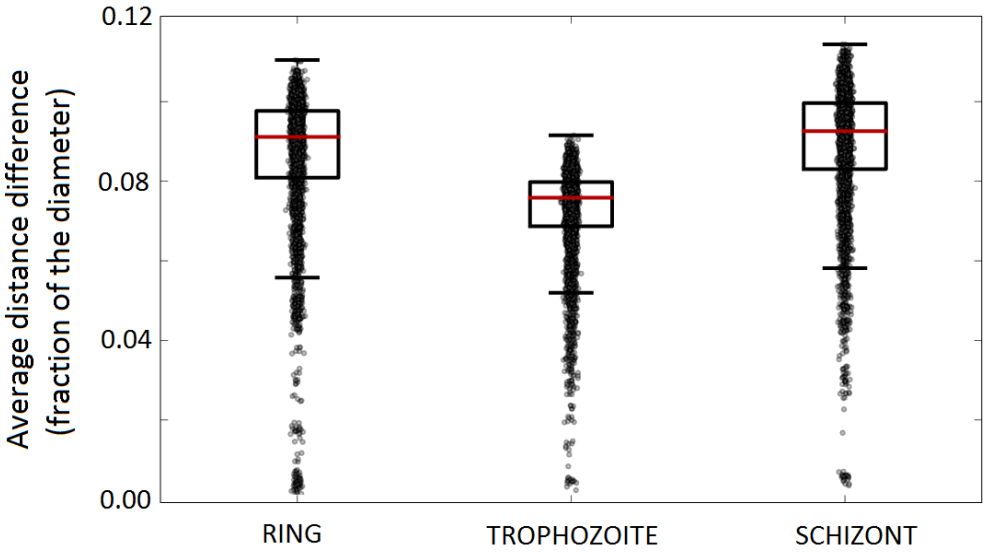

Supplementary Figure 4: **Similarity between 3D models inferred from 100 different initializations.**

We computed the average distance differences (Methods) for each pair of structures (i.e., $\binom{100}{2}$) that are inferred from different initializations and summarized these difference using a box plot for each stage. Each box extends from the lower to upper quartile values with a red line at the median. These results show that the 3D distance between a pair of loci varies, on the average, less than 10% of the nuclear diameter from one structure to another.

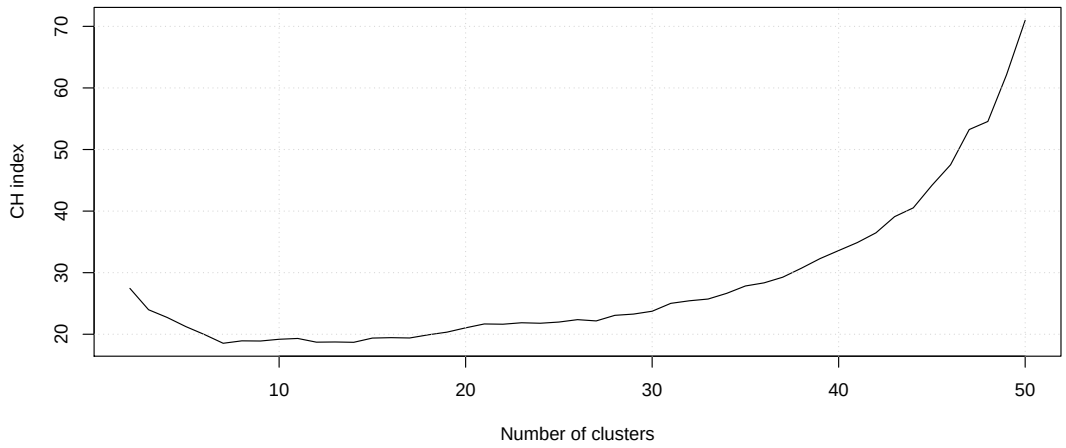

(a) Ring

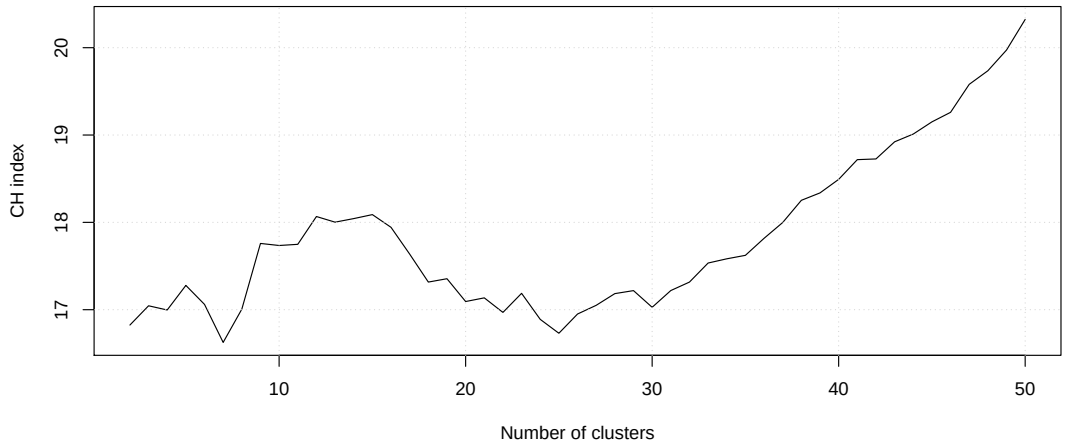

(b) Trophozoite

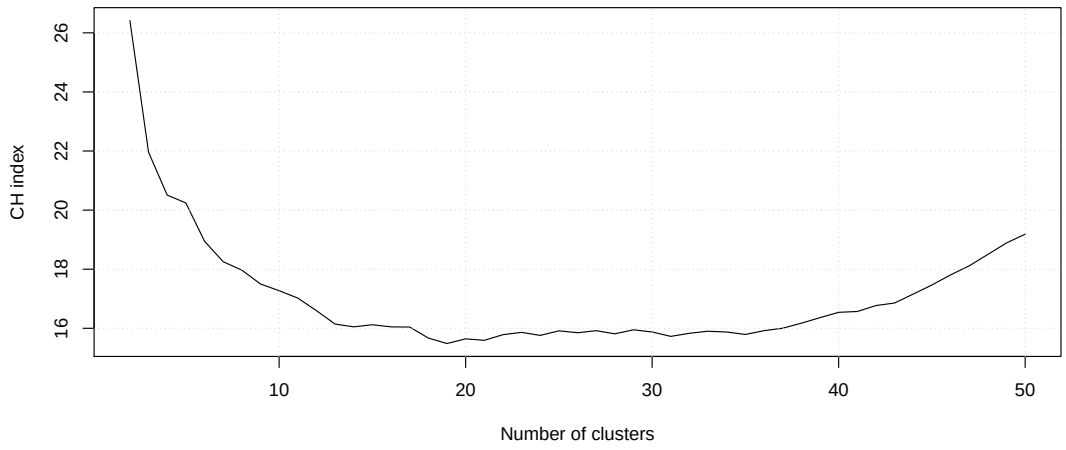

(c) Schizont

Supplementary Figure 5: **Clustering of the 100 structures using pairwise RMSD values.** To assess whether the 100 structures generated from different random initializations fall into discrete clusters we performed hierarchical clustering on the pairwise RMSD matrix of each stage. We computed and plotted the Calinski-Harabasz (CH) index [9] for each clustering while varying the number of clusters from 2 to 50. None of the stages exhibited a clear peak of the CH index, suggesting that the set of structures do not fall into discrete clusters.

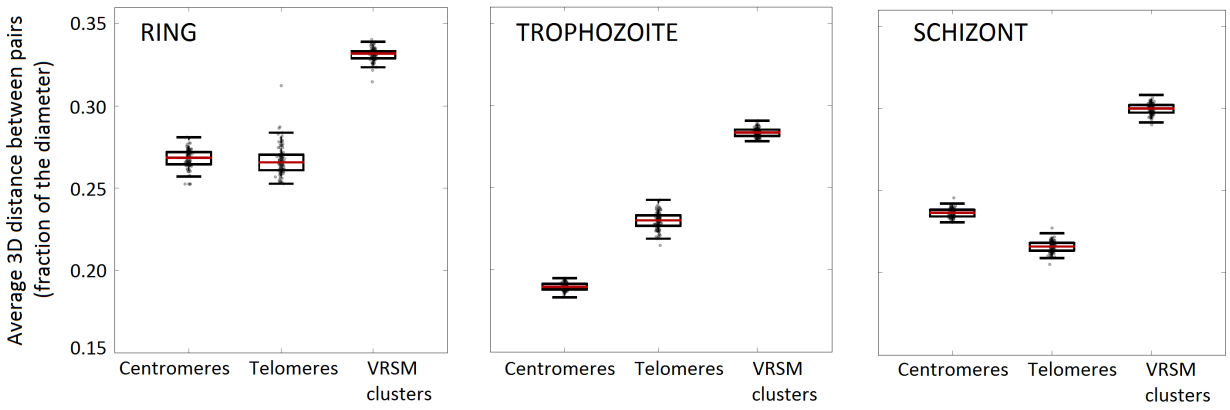

Supplementary Figure 6: **Conservation of centromere, telomere and VRSM gene colocalizations across 100 different initializations.**
We computed the average 3D distance between pairs of centromeres ($\binom{14}{2}$ pairs), telomeres ($\binom{28}{2}$ pairs) and VRSM clusters (8 internal, 28 subtelomeric clusters and a total of $\binom{36}{2}$ pairs) for each of the 100 structures inferred from different initializations and summarized these average distances using a box plot for each stage. Each box extends from the lower to upper quartile values with a red line at the median. These results suggest that the major organizational hallmarks concerning colocalization of centromere, telomere and VRSM gene regions are common to all structures gathered from different initializations.

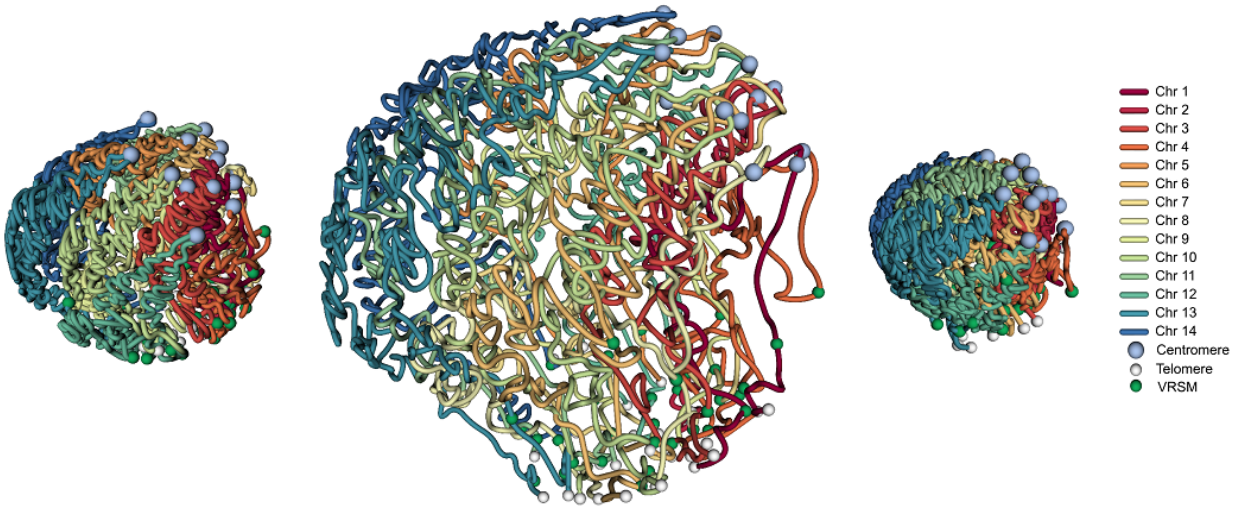

Supplementary Figure 7: **3D structures of all three stages (centromere clustering).**
This figure is identical to Main Figure 2a except the view is rotated to visualize the centromere clustering for each stage. Centromeres and telomeres are indicated with light blue and white spheres, respectively. Midpoints of VRSM gene clusters are shown with green spheres.

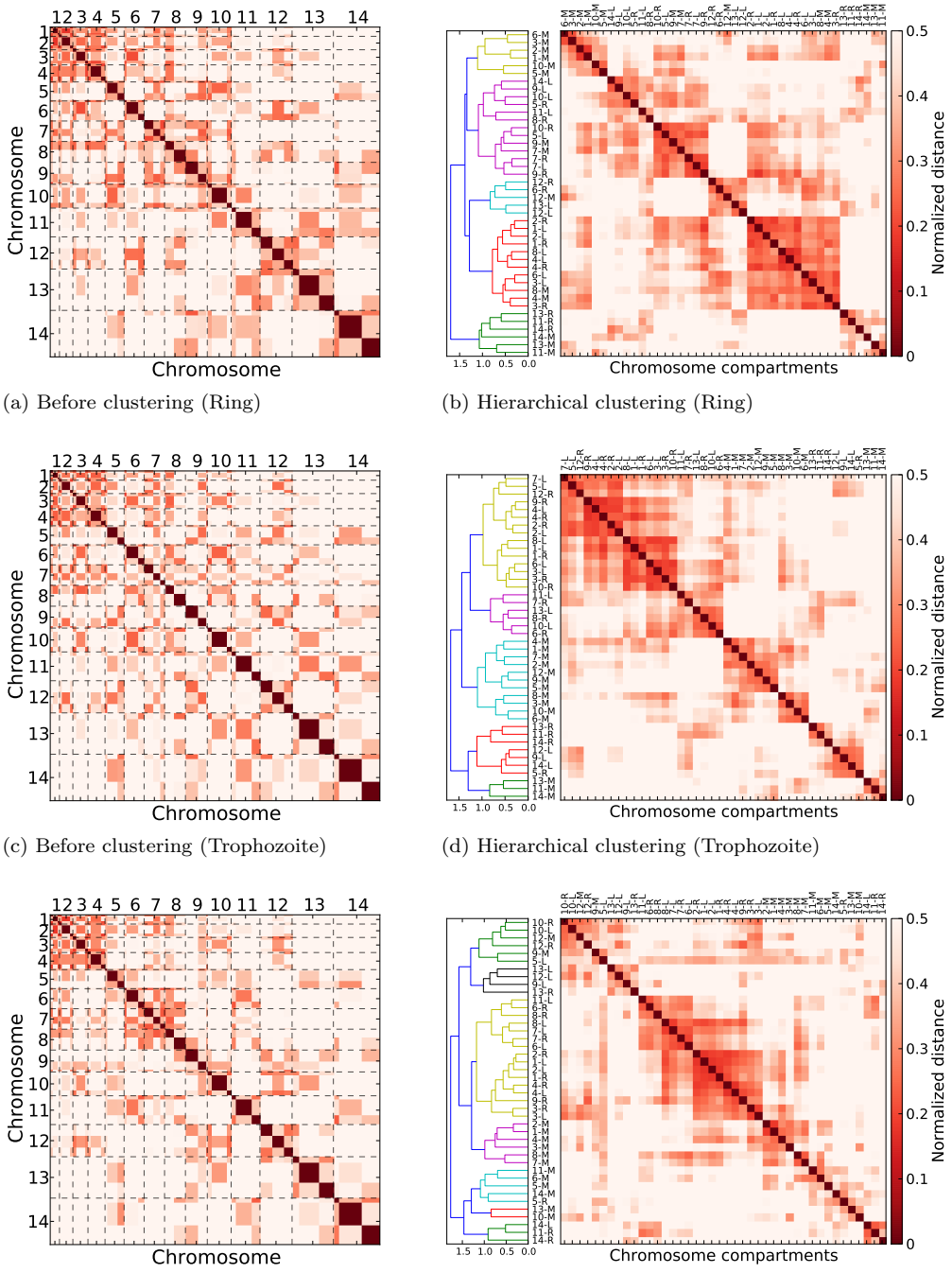

(a) Before clustering (Ring)

(b) Hierarchical clustering (Ring)

(c) Before clustering (Trophozoite)

(d) Hierarchical clustering (Trophozoite)

(e) Before clustering (Schizont)

(f) Hierarchical clustering (Schizont)

Supplementary Figure 8: **Hierarchical clustering of compartment distance matrices.** Pairwise compartment distance matrices (42×42, three compartments on each chromosome) that are identified by eigenvalue decomposition (Methods) for (a) ring, (c) trophozoite and (e) schizont stages. Distances are averaged over all pairs of loci between the two compartments and normalized using nuclear diameter to result in a fraction between 0 and 1. In the figure, the actual length of each compartment and each chromosome are preserved. Each compartment is colored separately, with dashed lines segregating adjacent chromosomes. Hierarchical clustering of pairwise compartment distance matrices for (b) ring, (d) trophozoite and (f) schizont stages. Clustering was performed using the average linkage score. Each compartment is represented by a fixed length, and L, M, R denote left, mid, right compartments, respectively. For all panels the color bars extend from 0 to 0.5 (i.e., distance equals nuclear radius).

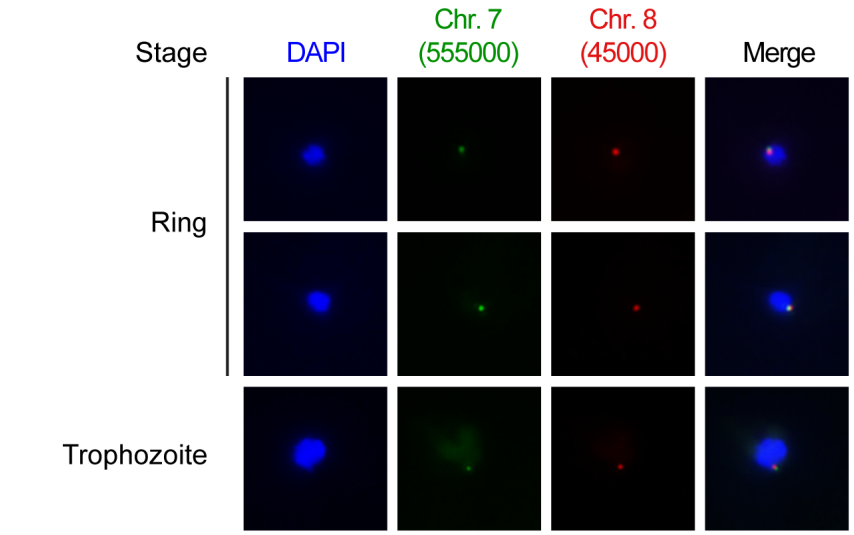

(a)

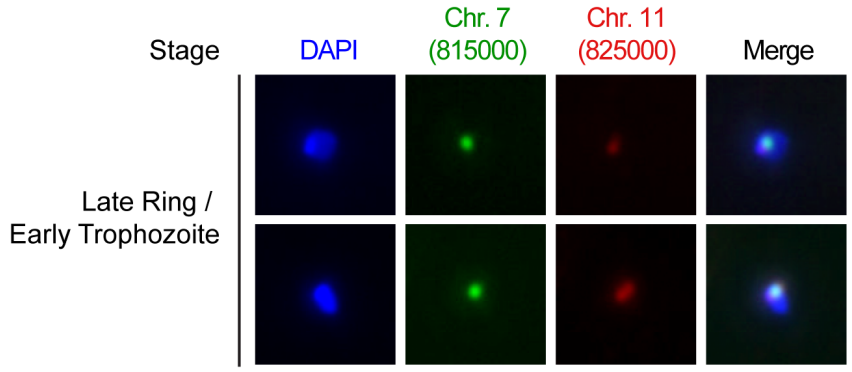

(b)

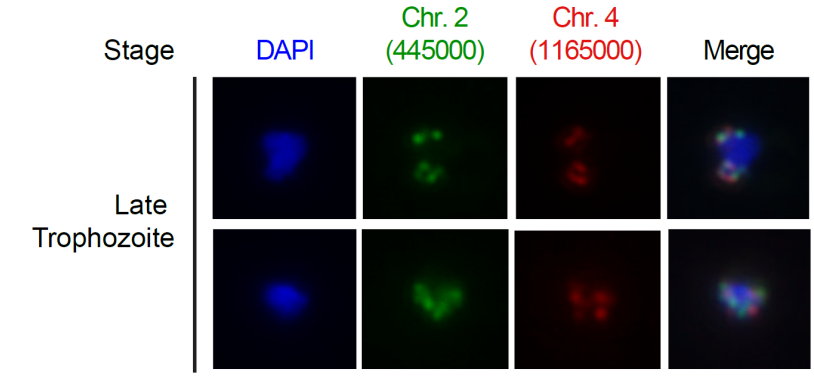

(c)

Supplementary Figure 9: Validation of 3D models with DNA FISH.
Additional FISH images for (a) a pair of interchromosomal loci with VRSM genes (chr7:550,000-560,000 containing internal VRSM genes and chr8:40,000-50,000 containing subtelomeric VRSM genes) (b) a pair of interchromosomal loci that harbor no VRSM genes (chr7:810,000-820,000 and chr11:820,000-830,000). (c) FISH images showing lack of colocalization as a negative control for a pair of interchromosomal loci that harbor no VRSM genes and have no contacts in trophozoite stage (chr2:440,000-450,000 and chr4:1,160,000-1,170,000).

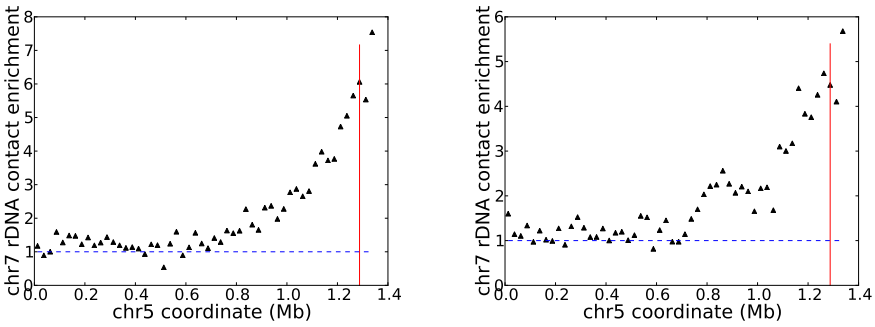

(a) Lemieux et al. data - DCJ On

(b) Lemieux et al. data - DCJ Off

(c) Lemieux et al. data - B15C2

(d) Lemieux et al. data - NF54 control

Supplementary Figure 10: **Clustering of highly transcribed rDNA units in Lemieux et al. data.** Hi-C libraries generated with MboI restriction enzyme from Lemieux et al. [10] were mapped to the *P. falciparum* genome and further processed using the pipeline we processed our data with to generate and normalize contact maps at 25 kb resolution. The normalized contact maps were used for virtual 4C plots using as a bait the A-type rDNA unit on chromosome 7. As suggested in Lemieux et al., contact counts from 50 kb up- and downstream of the 25 kb bin containing rDNA unit were used, and the rDNA-containing window itself was removed from the analysis. For each window w on chromosome 5, the contact enrichment was calculated by dividing the contact count between the bait and w to the average interchromosomal contact count for the bait locus.

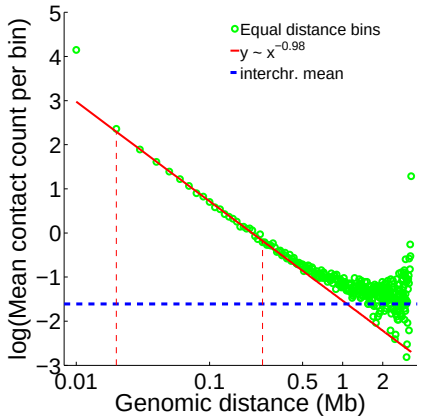

(a) Lemieux et al. data - B15C2

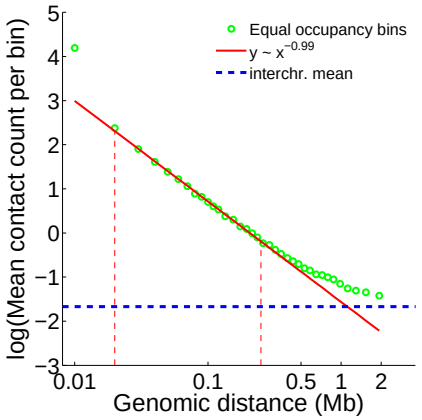

(b) Lemieux et al. data - B15C2

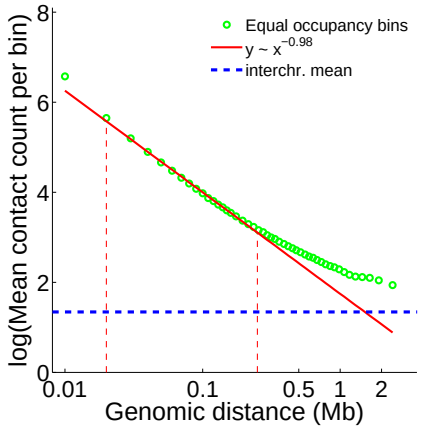

(c) Our data - Ring

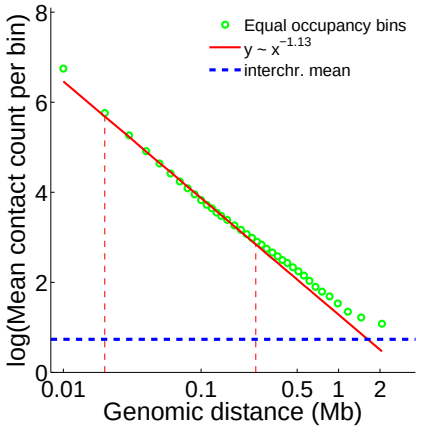

(d) Our data - Trophozoite

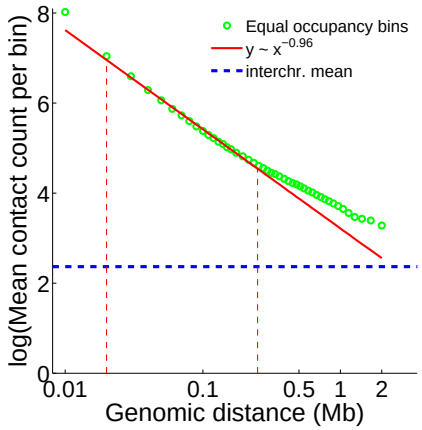

(e) Our data - Schizont

Supplementary Figure 11: **Comparison of inter and intrachromosomal contact prevalence.** The relationship between contact count and genomic distance is estimated using bins with equal genomic distances (e.g., 10 kb, 20 kb) in Lemieux et al. [10]. Due to the diminishing number of possible locus pairs with increasing genomic distance (e.g., only one locus pair for the bin with the largest genomic distance) this estimation leads to many high variance bins for large genomic distances. This issue can be addressed by using variable-width bins that contain equal numbers of contacts (see Methods). Plotted are the log (base e) of mean contact count per bin when using (a) equal distance binning, (b) equal occupancy binning for B15C2 library of Lemieux et al. [10] and (c-e) equal occupancy binning for ring, trophozoite and schizont stage data from this work. Dashed vertical red lines denote the range used to compute the log-linear fit.

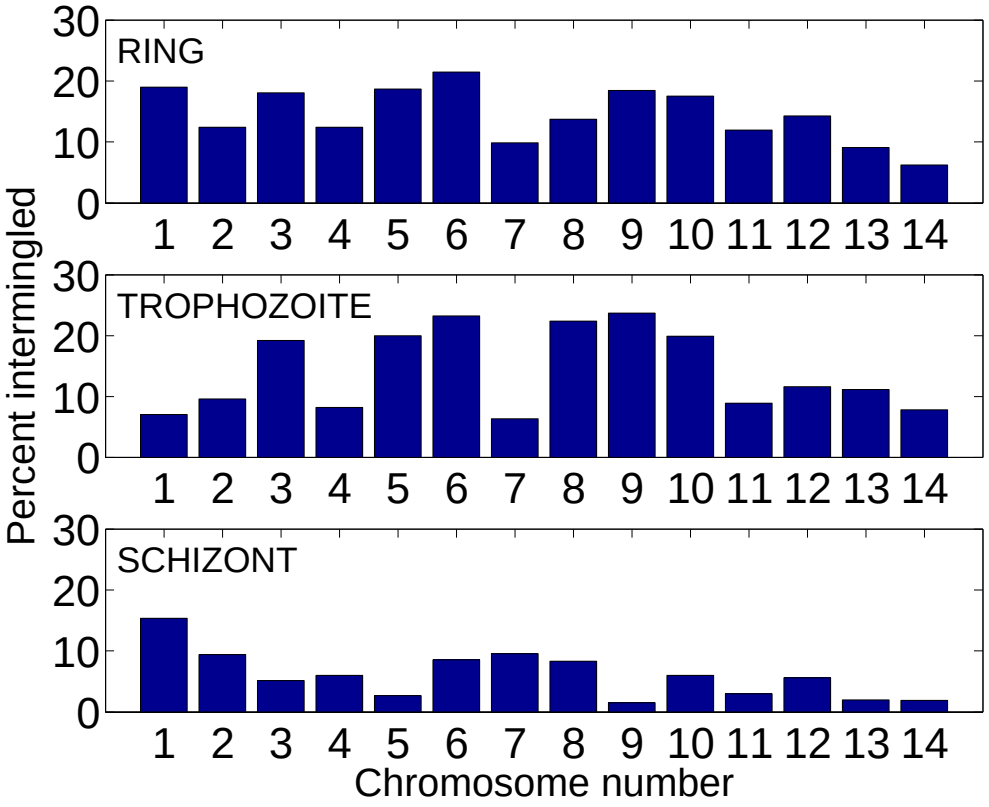

Supplementary Figure 12: **Changes in chromosome territories during the erythrocytic cycle.** The extent to which a chromosome intermingles with other chromosomes is characterized by the percentage of nuclear volume that is jointly occupied by the chromosome of interest and at least one other chromosome, relative to the entire volume occupied by the chromosome. To compute the percentages on the y-axis, the nuclear volume was sampled using 1,000,000 randomly generated small spheres with radius 5% of the actual nuclear radius. For each chromosome i, two numbers were calculated: the number of spheres that contain a locus from chromosome i (n_i) and the number of such spheres that contain no locus from another chromosome (e_i). The percent intermingled (y-axis) for chromosome i is computed as $100 \times \frac{n_i - e_i}{n_i}$. Because the exact percentages are highly dependent on the selection of the random sphere size, the procedure was repeated using spheres with radii 2%, 10% and 20% of the nuclear volume. For each setting, the trophozoite stage exhibited the highest amount of intermingling, whereas the schizont stage showed the lowest. Also, the larger chromosomes (i.e., chromosomes with higher numbers) consistently showed lower intermingling compared to smaller chromosomes at each stage and for each threshold.

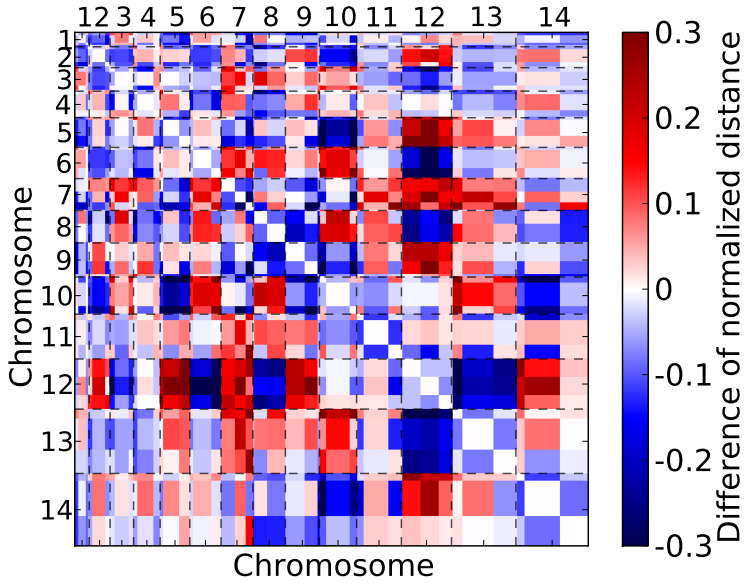

(a) From ring to trophozoite

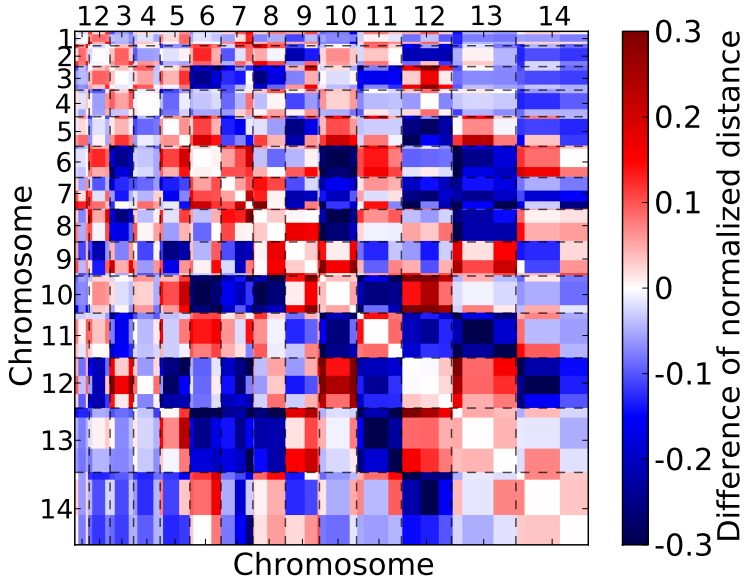

(b) From trophozoite to schizont

Supplementary Figure 13: **Movement of chromosome compartments with respect to each other.** Each compartment movement matrix is generated by subtracting the pairwise compartment distance matrix (Supplementary Fig. 8) of one stage from the matrix of the preceding stage. Plotted are the movements (a) from ring to trophozoite (i.e., trophozoite minus ring), (b) from trophozoite to schizont (i.e., schizont minus trophozoite). Red color indicates that a pair of compartments are closer in the later stage compared to the earlier, and blue color indicates vice versa.

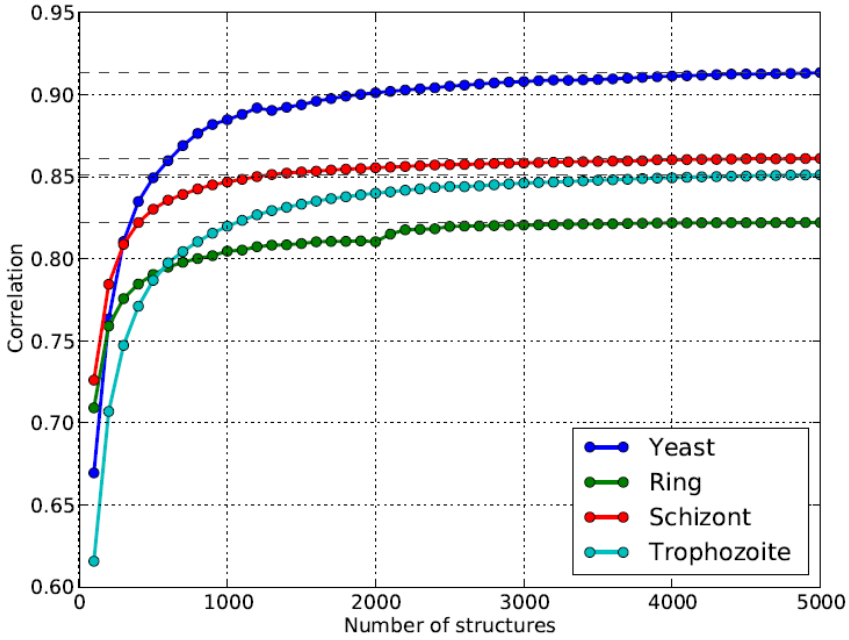

(a)

Contact map 1	*Contact map 2*	*Row-based corr.*	*Normalized row-based corr.*
Yeast *(Hi-C)[1]*	Yeast *(VE)*	0.915	0.573
	Yeast *(expected)*	0.922	0.115
Ring *(Hi-C)*	Ring *(VE)*	0.843	0.340
	Ring *(expected)*	0.928	0.072
Trophozoite *(Hi-C)*	Trophozoite *(VE)*	0.848	0.392
	Trophozoite *(expected)*	0.908	0.063
Schizont *(Hi-C)*	Schizont *(VE)*	0.864	0.487
	Schizont *(expected)*	0.923	0.081

(b)

Supplementary Figure 14: **Volume exclusion modeling and correlation calculation.** (a) Row-based Pearson correlation between the observed Hi-C contact map and the average contact map from volume exclusion modeling as a function of the number of simulated structures. (b) Row-based Pearson correlation and normalized row-based Pearson correlation between the two contact maps listed in each row for various Hi-C libraries. *VE* refers to contact maps obtained from 5000 structures generated by volume exclusion and *expected* refers to matrices with expected contact counts generated from observed *Hi-C* matrices as described in Methods.

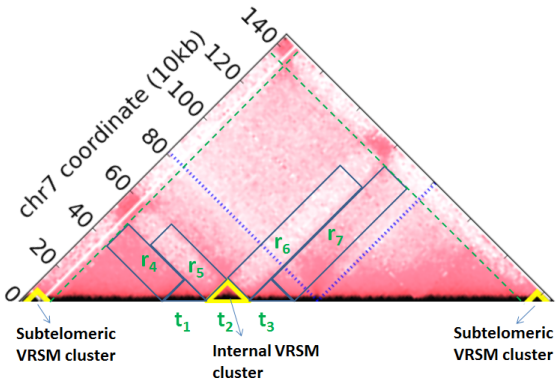

(a)

Internal VRSM	*Stage*	t_2 vs. t_1	t_2 vs. t_3	r_5 vs. r_4	r_6 vs. r_7
	R	0	0.7	0	-0.09
chr4(1)	T	0.06	0.2	-0.11	-0.25
	S	0.1	0.16	0.13	-0.14
	R	0.13	0.12	-0.38	-0.27
chr4(2)	T	0.15	0.15	-0.42	-0.33
	S	0.14	0.13	-0.37	-0.3
	R	0.03	0.08	-0.37	-0.34
chr4(3)	T	0.03	0.06	-0.55	-0.41
	S	0.03	0.01	-0.48	-0.42
	R	0.12	0.1	0.02	-0.06
chr6(1)	T	0.19	0.2	-0.09	-0.16
	S	0.16	0.18	-0.08	-0.14
	R	0.11	0.2	-0.19	-0.18
chr7(1)	T	0.19	0.28	-0.36	-0.3
	S	0.08	0.19	-0.27	-0.27
	R	0.15	0.08	-0.05	-0.09
chr8(1)	T	0.17	0.09	-0.17	-0.13
	S	0.14	0.09	-0.11	-0.11
	R	0.07	0.05	-0.02	-0.01
chr12(1)	T	0.05	0.14	-0.04	-0.02
	S	0.09	0.12	-0.07	-0.08
	R	0.09	0.09	-0.09	-0.11
chr12(2)	T	0.17	0.1	-0.27	-0.24
	S	0.09	0.07	-0.19	-0.23

(b)

Supplementary Figure 15: **Quantification of domain-like behavior of VRSM gene clusters.** (a) Each internal VRSM gene cluster is characterized by a set of strong intra-cluster contacts (t_2) and two sets of contacts with adjacent regions (r_5 and r_6) that are weak. For comparison, we also consider flanking, non-VSRM regions of the same size as the original VRSM cluster, including their "intra-cluster" contacts (t_1 and t_3) which should be similar to t_2 for a contact map without domain-like structures around VRSM clusters and contacts with adjacent regions (r_4 and r_7) which are comparable to (r_5 and r_6). As seen in this example, a domain-like structure for a VRSM cluster leads to stronger contacts (+ sign) within t_2 compared to both t_1 and t_3, and weaker contacts (- sign) within r_4 and r_7 compared to r_5 and r_6. (b) The table reports, for each internal VRSM gene cluster and each stage, the average normalized difference between the intra-cluster contacts within the cluster compared to its two flanking control regions, and similarly for the contacts with adjacent regions. The metric we use for comparing two contact sub-matrices X, Y of dimension $N \times M$ is $\frac{1}{NM}\sum_{i=1}^{N}\sum_{j=1}^{M}\frac{x_{ij}-y_{ij}}{\frac{1}{2}(x_{ij}+y_{ij})}$ where x_{ij} and y_{ij} are the ijth entries of X and Y, respectively. Values that have signs inconsistent with the expected pattern (i.e., +, +, -, -) are indicated with a grey background. Every internal VRSM cluster exhibits the expected sign pattern in at least one stage.

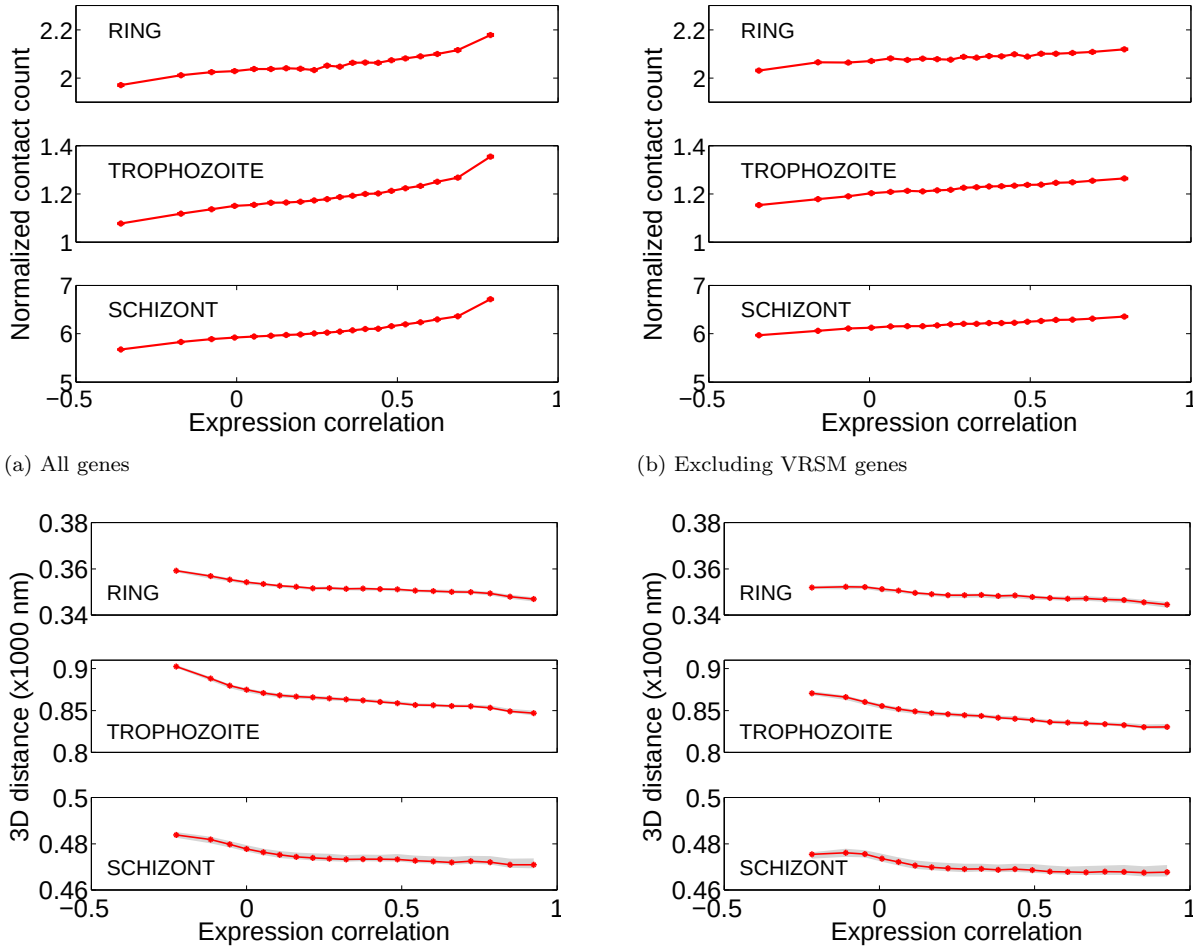

(a) All genes

(b) Excluding VRSM genes

(c) All genes

(d) Excluding VRSM genes

Supplementary Figure 16: **Revisiting the relationship between 3D architecture and gene expression by excluding VRSM genes.**
(a) is identical to Main Figure 6a and (b) is generated identical to (a) except all gene pairs involving at least one VRSM gene are omitted from the analysis. Re-evaluation of our hypothesis that interchromosomal gene pairs that have contact counts within the top 20% for each stage have more highly correlated expression profiles than the remaining gene pairs still yielded significant p-values for each stage [Wilcoxon rank-sum test, p-values 1.07e-70 (ring), 0 (trophozoite), and 1.68e-302 (schizont)]. (c) is identical to Main Figure 6b and (d) is generated identical to (c) except all gene pairs involving at least one VRSM gene are omitted from the analysis. Re-evaluation of our hypothesis that interchromosomal gene pairs closer than 20% of the nuclear diameter have more highly correlated expression profiles than other genes still yielded significant p-values for each stage [Wilcoxon rank-sum test, p-values 3.27e-48 (ring), 1.32e-157 (trophozoite), and 2.16e-5 (schizont)].

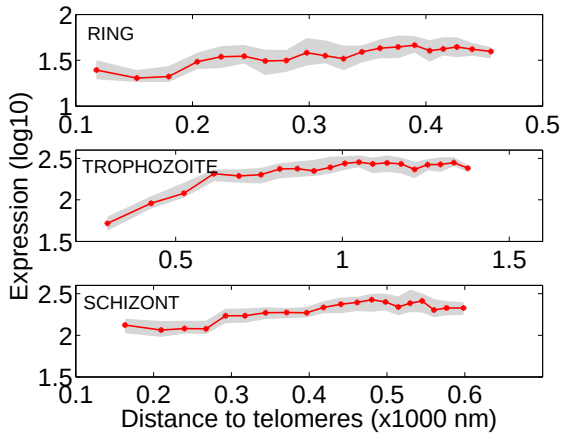

(a) All genes

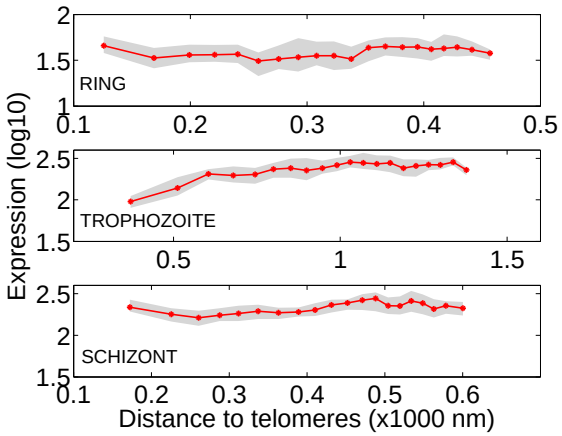

(b) Excluding VRSM genes

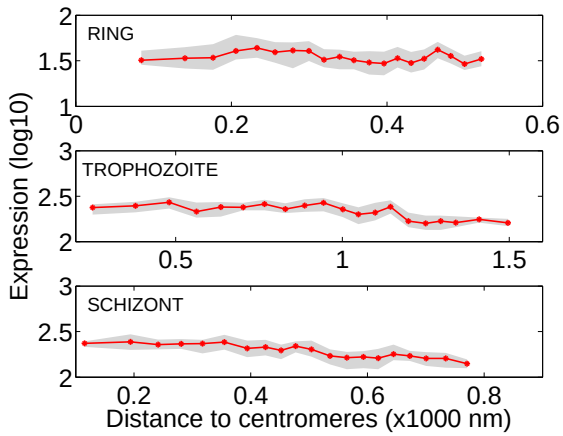

(c) All genes

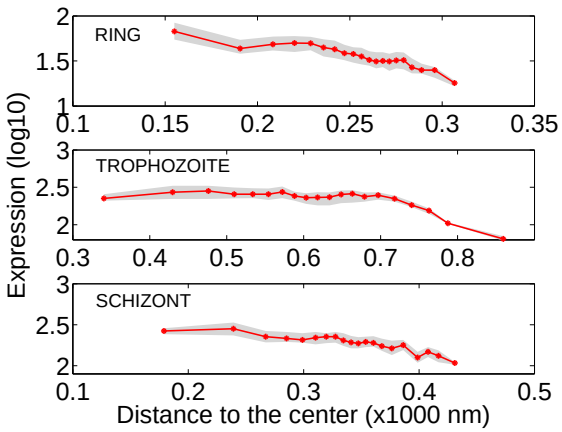

(d) All genes

Supplementary Figure 17: **The relationship between distance to the telomeres, nuclear center and centromeres versus the gene expression.**
(a) is identical to Main Figure 6c and (b) is generated identical to (a) except all VRSM genes are omitted from the analysis. Re-evaluation of our hypothesis that genes which lie within a distance of 20% of the nuclear diameter to the centroid of the telomeres exhibit lower expression levels yielded a significant p-value for trophozoite stage but not for ring and schizont stages at a significance threshold of 0.01 [Wilcoxon rank-sum test, p-values 0.21 (ring), 1.5e-3 (trophozoite), and 0.035 (schizont)]. (c) and (d) are generated identical to (a) expect the distance of genes are measured to (c) the centroid of the centromeres and (d) the nuclear center. For each figure, genes are first sorted in increasing order according to their distances to the landmark of interest and then binned into 20 equal width quantiles (5th, 10th, ..., 100th). For each bin, the average distance to the landmark (x-axis) and the average log expression value [11] together with its standard error (y-axis) are computed and plotted.

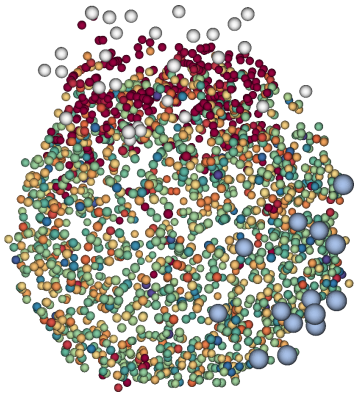

(a) First component (Ring)

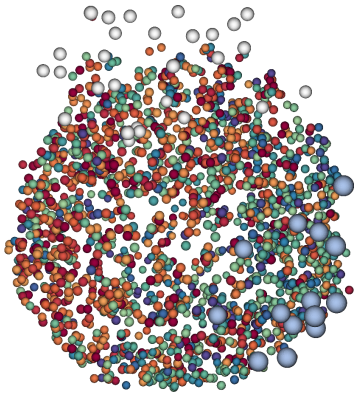

(b) Second component (Ring)

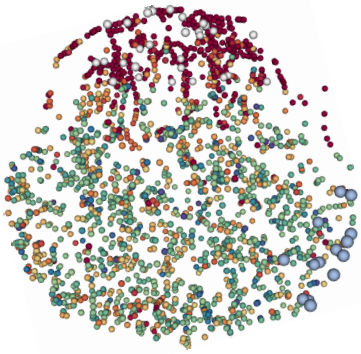

(c) First component (Trophozoite)

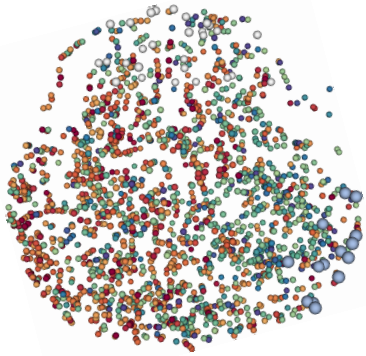

(d) Second component (Trophozoite)

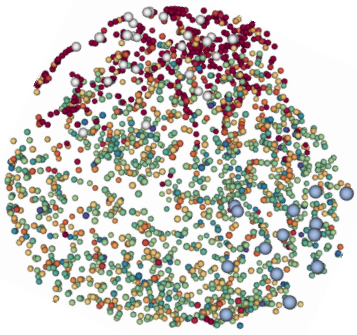

(e) First component (Schizont)

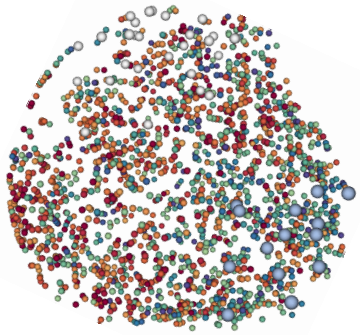

(f) Second component (Schizont)

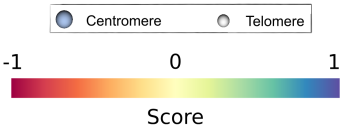

Supplementary Figure 18: **kCCA expression profiles component score.**
Each panel shows the projection of the gene expression profile onto one of the two extracted kCCA profiles for a specified erythrocytic stage, with the score of the projection encoded on the color scale. For the first kCCA component, the projections consistently exhibit a striking gradient from the telomeric region across the nucleus, while for the second component, which is less coherent with the 3D structure, the projection gradient extends from the centromeres across the nucleus.

Supplementary Notes

Supplementary Note 1: Tethered conformation capture procedure

Day 1 Parasite pellets were thawed on ice in 550 μl Hi-C lysis buffer (25 mM Tris-HCl at pH 8.0, 10 mM NaCl, 2 mM AEBSF, Roche Complete Mini EDTA-free protease inhibitor cocktail [Roche, Basel, Switzerland], 0.25% Igepal CA-630) per 140 mg. Parasite membranes were disrupted by passing the lysate through a 26.5 gauge needle 15 times using a syringe. Samples were spun at 2,500 $\times$ g for 5 min at room temperature (RT). Pellets were washed twice with 1 ml ice-cold wash buffer (50 mM Tris-HCl at pH 8.0, 50 mM NaCl, 1 mM EDTA) and resuspended in the same buffer to a final volume of 250 μl. Samples were mixed with 95 μl 2% SDS to a final concentration of 0.5% and incubated at 55°C for 15 min. Suspensions were cooled down to RT before they were mixed with 105 μl 25 mM EZ-link Iodoacetyl-PEG2-Biotin (IPB) (Thermo Fisher Scientific, Waltham, MA, USA) to biotinylate proteins. After incubating for 1 h at RT while rotating, the SDS was neutralized by adding 1.3 ml 1$\times$ NEBuffer 2 (New England Biolabs [NEB], Ipswich, MA, USA). Samples were mixed with 225 μl 10% Triton X-100 to a final concentration of 1% and incubated for 10 min on ice, followed by 10 min at 37°C. Five μl 1 M DTT, 100 μl 10$\times$ NEBuffer 2, 415 μl water and 35 μl MboI restriction enzyme (NEB) (25 units/μl) was added to digest the DNA overnight at 37°C in a total volume of 2,530 μl.

Day 2 After digestion, samples were loaded into a Slide-A-Lyzer Dialysis Cassette G2 (Thermo Fisher Scientific) and dialyzed for 4 h at RT against 1 L of dialysis buffer (10 mM Tris-HCl at pH 8.0, 1 mM EDTA) to eliminate excess IPB remaining from the biotinylation step. Dialysis buffer was renewed after 3 h. Four hundred μl MyOne Streptavidin T1 beads (Life Technologies, Carlsbad, CA, USA) were washed 3 times with PBS + 0.01% Tween-20 (PBST) and beads were resuspended in 2 ml PBST. Dialyzed samples were divided into 5 equal aliquots of 500 μl in 1.7 ml prelubricated microcentrifuge tubes (Corning, Corning, NY, USA). Four hundred μl beads were added to each tube and samples were incubated for 30 min at RT while rotating. To prevent interference of unbound streptavidin on the beads with later steps (adding biotinylated dCTP) 5 μl neutralized IPB was added to each tube. IPB was neutralized by adding an equimolar amount of 2-mercaptoethanol. Samples were incubated for an additional 15 min at RT while rotating. Not biotinylated chromatin and not cross-linked DNA was removed by washing the magnetic T1 beads once with 600 μl PBST and once with 600 μl wash buffer (10 mM Tris-HCl at pH 8.0, 50 mM NaCl, 0.4% Triton X-100). Beads were resuspended in 100 μl of the same wash buffer. MboI generated 5$'$ overhangs were filled in by adding 63 μl water, 1 μl 1 M MgCl, 10 μl 10$\times$ NEBuffer 2, 0.7 μl 10 mM dATP, 0.7 μl 10 mM dTTP, 0.7 μl 10 mM 2'-Deoxyguanosine-5'-O-(1-thiotriphosphate), sodium salt, Sp-isomer (Axxora, San Diego, CA, USA), 15 μl 0.4 mM Biotin-14-dCTP (Life Technologies), 4 μl 10% Triton X-100 and 5 μl 5U/μl DNA Polymerase I, Large (Klenow) Fragment (NEB). Samples were incubated for 40 min at RT while rotating. Reaction was stopped by adding 5 μl 0.5 M EDTA to the suspension. After 2 min of incubation at RT while rotating, beads were washed twice with 600 μl buffer (50 mM Tris-HCl at pH 7.4, 0.4% Triton X-100, 0.1 mM EDTA) and resuspended in 500 μl of the same buffer. Each sample was transferred into a 15 ml centrifuge tube. For blunt-end ligation under dilute conditions 500 μl sample was mixed with 4 ml water, 250 μl 10$\times$ Ligase Buffer (NEB), 100 μl 1 M Tris-HCl at pH 7.4, 90 μl 20% Triton X-100, 50 μl 100$\times$ BSA and 2 μl 2,000 U/μl T4 DNA Ligase (NEB), and incubated overnight at 16°C.

Day 3 The ligation reaction was stopped by adding 200 μl 0.5 M EDTA to each of the five 15 ml tubes. The magnetic T1 beads were collected on the wall of the tube using a magnet and the solution was aspirated out of the tube. The beads were resuspended in 400 μl extraction buffer (50 mM Tris-HCl at pH 8.0, 0.2% SDS, 1 mM EDTA, 500 mM NaCl) and the mix was transferred into a new microcentrifuge tube. Samples were treated with 5 μl RNase A (20 mg/ml) (Life Technologies) for 45 min at 37°C and with 20 μl Proteinase K (20 mg/ml) (NEB) overnight at 45°C.

Day 4 An additional 5 μl Proteinase K was added and samples were incubated for another 2 h at 45°C. Beads were collected on the wall of the tube and DNA was extracted from the supernatant twice with an

equal volume of phenol:chloroform:isoamyl alcohol (25:24:1) and once with an equal volume of chloroform. The aqueous phase was mixed with sodium chloride and glycogen to a final concentration of 200 mM and 25 μg/ml, respectively. DNA was precipitated by adding 900 μl ice-cold 200 proof pure ethanol and incubation at -20°C overnight or at -80°C for $>$ 1 h. Precipitated DNA was pelleted by centrifugation at 16,100 $\times$ g for 30 min at 4°C. Pellets were washed with ice-cold 80% ethanol, spun down at 16,100 $\times$ g for 15 min at 4°C and resuspended in 20 μl 10 mM Tris-HCl at pH 8.0.

Day 5 Two to five μg purified DNA was treated with Exonuclease III (NEB) (60 units per μg DNA) in 120 μl 1$\times$ NEBuffer 1 for one h at 37°C. The reaction was ended by adding 2.7 μl 0.5 M EDTA and 2.7 μl 5 M NaCl, and subsequent incubation at 70°C for 20 min. DNA was transferred into TPX microtubes (Diagenode, Denville, NJ, USA) and sonicated using a Bioruptor UCD-200 (Diagenode) at high intensity for 30 min using 30 sec on, 30 sec off cycles. Agencourt AMPure XP beads (Beckman Coulter, Brea, CA, USA) were used to purify DNA, which was eluted in 50 μl water.

Day 6 All amounts mentioned for subsequent end-repair and adding of A-overhangs are per μg of DNA used as input at the start of Day 5. DNA ends were repaired by treating the DNA with 1 U of DNA Polymerase I, Large (Klenow) Fragment (NEB), 3 U of T4 DNA Polymerase (NEB), 10 U of T4 Polynucleotide Kinase (NEB) in 100 μl 1$\times$ T4 DNA Ligase Buffer (NEB) with 0.4 mM of dNTPs for 30 min at 20°C. Importantly, T4 DNA Polymerase and not T4 DNA Ligase should be used for end-repair (Reza Kalhor, personal communication). This was apparently written incorrectly in the original TCC protocol [2]. DNA was purified using magnetic beads and eluted in 40 μl water. A-overhangs were added by treating the DNA with 3 U of Klenow Fragment ($3' \rightarrow 5'$ exo–) (NEB) in 50 μl 1$\times$ NEBuffer 2 with 0.2 mM dATP for 30 min at 37°C. The reaction was ended by adding 1 μl of 0.5 M EDTA. Ten μl of MyOne Streptavidin C1 magnetic beads (Invitrogen) were washed twice with 500 μl 1$\times$ Bind & Wash (B&W) buffer (5 mM Tris-HCl at pH 7.4, 0.5 mM EDTA, 1 M NaCl) and resuspended in 50 μl 2$\times$ B&W buffer. The DNA sample and the C1 beads were mixed and incubated at RT for 30 min. The beads were washed once with 500 μl 1$\times$ B&W buffer with 0.1% Triton, once with 500 μl 10 mM Tris-HCl at pH 8.0 and were resuspended in 10 μl water.

The Encore NGS Multiplex System (Nugen, San Carlos, CA, USA) was used for adapter ligation and library preparation of the cross-linked and non-cross-linked trophozoite samples. Amplification conditions were 45 sec at 98°C, 5 cycles of 15 sec at 98°C, 30 sec at 55°C and 30 sec at 62°C, followed by 10 cycles of 15 sec at 98°C, 30 sec at 63°C and 30 sec at 72°C, and a final elongation of 5 min at 72°C. NEBNext Multiplex Oligos for Illumina (NEB) and NEBNext Library Prep Reagents Set (NEB) were used for adapter ligation and library preparation of the ring and schizont samples. Amplification conditions were 45 sec at 98°C, 8 cycles of 15 sec at 98°C, 30 sec at 55°C and 30 sec at 62°C, followed by 3 cycles of 15 sec at 98°C, 30 sec at 63°C and 30 sec at 72°C, and a final elongation of 5 min at 72°C. KAPA HiFi DNA Polymerase HotStart ReadyMix (Kapa Biosystems, Woburn, MA, USA) was used for all PCRs. DNA in the supernatant was purified with Agencourt AMPure XP beads. Library quantification was performed using a 2100 Bioanalyzer (Agilent Technologies, Santa Clara, CA, USA). Libraries were subsequenctly sequenced on a HiSeq 2000 system (Illumina, San Diego, CA, USA) at the Institute for Integrative Genome Biology (University of California, Riverside, USA), generating 50 bp paired-end sequence reads.

Supplementary Note 2: Assigning statistical significance to normalized contact maps

We can describe our confidence estimation procedure as follows. Let N_{inter}, N_{intra} denote the total number of observed informative paired-end reads between inter and intrachromosomal locus pairs and M_{inter}, M_{intra} denote the number of such inter and intrachromosomal locus pairs, respectively. If we assume that an observed paired-end read is equally likely to come from any locus pair, then the null probability that the read comes from a specific locus pair is $p_{inter} = \frac{1}{M_{inter}}$ and $p_{intra} = \frac{1}{M_{intra}}$ for intrachromosomal and interchromosomal pairs, respectively. We use a previously described iterative procedure [8] to estimate

locus-specific biases and adjust the interchromosomal probability accordingly: $\bar{p}_{ij} = p_{inter} * B_i * B_j$, where B_i and B_j are the estimate bias terms.

For intrachromosomal locus pairs the assumption that each read is equally likely to come from any locus pair fails due to the significant effect of genomic distance on the contact probability. To account for this effect, we used a method that estimates the prior contact probability between two loci given their genomic distance by fitting a smooth spline and refining the underlying null distribution of contact probabilities [12]. For intrachromosomal locus pair (ℓ_i, ℓ_j) with genomic distance d, this spline is used to estimate the contact probability $p_{intra}(d)$. Similar to the interchromosomal pairs, this probability is corrected for biases of each locus ℓ_i and ℓ_j resulting in $\bar{p}_{ij} = p_{intra}(d) * B_i * B_j$.

Once the corrected null probabilities $\bar{p}_{ij}$ are computed for each possible inter and intrachromosomal locus pair, we computed the significance of observing k_{ij} informative reads between (ℓ_i, ℓ_j) among either $N = N_{inter}$ or $N = N_{intra}$ total reads, depending on the contact type. Dropping the subscripts from $\bar{p}_{ij}$ and k_{ij}, we calculated the significance as the p-value from the binomial distribution:

$$p(K \geq k) = \sum_{i=k}^{N} \Pr(K = i) \tag{1}$$

where

$$\Pr(K = k) = \binom{N}{k} \bar{p}^k \left(1 - \bar{p}\right)^{N-k}.$$

Finally, we corrected the combined collection of p-values for multiple testing by estimating, for a given p-value threshold, the proportion of false positive contacts with p-values below the threshold. This proportion is known as the *false discovery rate* (FDR), which can be estimated using standard methods [4].

Supplementary Note 3: DNA-FISH

DNA-FISH experiments were performed according to a recently published protocol [13] with minor modifications. P. falciparum-infected erythrocytes were pelleted by centrifuging at 800 × g for 5 min at 4°C, with minimal braking (brake = 1). To lyse erythrocyte membranes, double sorbitol-synchronized ring and trophozoite stage parasites were treated with 5 volumes of 0.015% cold saponin in cold PBS on ice for 20 or 10 min, respectively. Parasites were spun down at 4,200 × g for 10 min at 4°C, with minimal braking, and washed up to 7 times (2,000 × g, 10 min, brake = 5) with cold PBS. Parasites were then resuspended 4% formaldehyde (in PBS at room temperature) and fixed on ice for 15 min. After this fixation, parasites were washed 2 times in cold PBS (4,200 × g, 1 min, maximum brake) and resuspended in cold PBS.

A monolayer of parasites was deposited within a 9 × 9 mm frame-seal slide chamber (Bio-Rad, Hercules, CA, USA) that was prepared on a standard microscopy slide, and slides were air-dried for 30 min at RT. The fixed, air-dried parasites were washed with PBS for 5 min at RT, treated with 0.1% Triton X-100 in PBS for 5 min at RT and washed twice with PBS for 5 min at RT. Hybridization solution (50% formamide, 10% dextran sulfate, 2 × SSPE, 250 μg/ml single-stranded DNA from salmon testes) containing the denatured (5 min at 95°C) probes was applied and slide chambers were covered with a coverslip. Slides were denatured at 80°C for 30 min followed by hybridization at 37°C overnight. After removal of the coverslip and the hybridization solution, slides were washed in 2 × SSC/50% formamide for 30 min at 37°C, followed by 1 × SSC for 10 min at 50°C, 2 × SSC for 10 min at 50°C and 4 × SSC for 10 min at 50°C. Parasites were equilibrated in M solution (100 mM maleic acid, 150 mM NaCl, 1% bovine serum albumin) set at neutral pH, for 5 min at RT in a humid chamber, protected from light. M solution was removed and replaced with M solution containing Avidin, NeutrAvidin, Rhodamine Red-X Conjugate (Life Technologies) (1:1,000) for detection of the biotin probes. Slides were incubated for 30 min at RT, in a humid chamber, protected from light, and subsequently washed 3 times in TNT solution (100 mM Tris-HCl at pH 7.5, 150 mM NaCl, 0.5% Tween 20) for 10 min at RT with agitation. Cells were stained with DAPI (0.5 μg/ml in TNT solution) for 2 - 3 seconds. Slides were then air-dried (protected from light) and mounted using gelvatol with 2.5% Dabco anti-fade (Sigma-Aldrich, St. Louis, MO, USA). Images were acquired using an Olympus BX40 epifluorescent microscope (Olympus, Center Valley, PA, USA).

Supplementary Note 4: Volume exclusion modeling

Tjong et al. show the budding yeast's dominant architectural features can be entirely explained by a simple volume exclusion model, modeling chromatin as a random flexible polymer with few biologically motivated architectural constraints [14]. Following their methodology, we computed a population of 5000 structures for the budding yeast using the same sets of constraints, and we successfully recovered high correlation between the contact maps generated from the population of structures and the observed Hi-C matrix (Supplementary Fig. 14(a)).

Even though the row-based correlation has been used as a measure of consistency between two contact maps [14, 8], we hypothesized that this measure may be dominated by the strong diagonal trend of contact maps and, hence, may not capture non-random similarity between two contact matrices. To test this hypothesis, we generated an *expected contact matrix* by setting each interchromosomal contact count to the expected contact count for its genomic distance, as defined in Methods. We obtained an even higher correlation between the observed Hi-C matrix and this structureless expectation matrix (Supplementary Fig. 14(b)).

To account for this problem, we developed a new scoring measure, the *normalized* row-based Pearson correlation, which replaces each count value with its ratio to an expected count in the correlation computation (Methods). Supplementary Fig. 14(b) demonstrates that the normalized row-based Pearson correlation is more effective for comparing contact maps: indeed, the correlations between structureless matrices (marked as *expected*) and observed Hi-C matrices are close to zero, while the correlations between the simulated (VE) and observed Hi-C contact matrices are conserved.

Supplementary References

[1] Z. Duan, M. Andronescu, K. Schutz, S. McIlwain, Y. J. Kim, C. Lee, J. Shendure, S. Fields, C. A. Blau, and W. S. Noble. A three-dimensional model of the yeast genome. *Nature*, 465:363–367, 2010. PMC2874121.

[2] R. Kalhor, H. Tjong, N. Jayathilaka, F. Alber, and L. Chen. Genome architectures revealed by tethered chromosome conformation capture and population-based modeling. *Nat Biotechnol*, 30(1):90–98, 2011.

[3] D. M. Witten and W. S. Noble. On the assessment of statistical significance of three-dimensional colocalization of sets of genomic elements. *Nucleic Acids Research*, 40(9):3849–3855, 2012. PMC3351188.

[4] Y. Benjamini and Y. Hochberg. Controlling the false discovery rate: a practical and powerful approach to multiple testing. *J R Stat Soc Series B*, 57:289–300, 1995.

[5] W. A. Hoeijmakers, C. Flueck, K. J. Francoijs, A. H. Smits, J. Wetzel, J. C. Volz, A. F. Cowman, T. Voss, H. G. Stunnenberg, and R. Bártfai. *Plasmodium falciparum* centromeres display a unique epigenetic makeup and cluster prior to and during schizogony. *Cell Microbiology*, 14(9):1391–1401, 2012.

[6] L. Mancio-Silva, Q. Zhang, C. Scheidig-Benatar, and A. Scherf. Clustering of dispersed ribosomal DNA and its role in gene regulation and chromosome-end associations in malaria parasites. *Proceedings of the National Academy of Sciences of the United States of America*, 107(34):15117–15122, 2010.

[7] K. G. Le Roch, Y. Zhou, P. L. Blair, M. Grainger, J. K. Moch, J. D. Haynes, P. de la Vega, A. A. Holder, S. Batalov, D. J. Carucci, and E. A. Winzeler. Discovery of gene function by expression profiling of the malaria parasite life cycle. *Science*, 301(5639):1503–1508, 2003.

[8] M. Imakaev, G. Fudenberg, R. P. McCord, N. Naumova, A. Goloborodko, B. R. Lajoie, J. Dekker, and L. A. Mirny. Iterative correction of Hi-C data reveals hallmarks of chromosome organization. *Nat Methods*, 9:999–1003, 2012.

[9] R.B. Calinski and J. Harabasz. A dendrite method for cluster analysis. *Comm. in Statistics*, 3:1–27, 1974.

[10] J. E. Lemieux, S. A. Kyes, T. D. Otto, A. I. Feller, R. T. Eastman, R. A. Pinches, M. Berriman, X. Z. Su, and C. I. Newbold. Genome-wide profiling of chromosome interactions in *Plasmodium falciparum* characterizes nuclear architecture and reconfigurations associated with antigenic variation. *Mol Microbiol*, 90(3):519–537, 2013.

[11] E. M. Bunnik, D. W. Chung, M. Hamilton, N. Ponts, A. Saraf, J. Prudhomme, L. Florens, and K. G. Le Roch. Polysome profiling reveals translational control of gene expression in the human malaria parasite *Plasmodium falciparum*. *Genome Biology*, 14(11):R128, 2013.

[12] F. Ay, T. L. Bailey, and W. S. Noble. Statistical confidence estimation for Hi-C data reveals regulatory chromatin contacts. *Genome Res*, doi:10.1101/gr.160374.113, 2014.

[13] M. Contreras-Dominguez, C. B. Moraes, T. Dorval, A. Genovesio, F. M. Dossin, and L. H. Freitas-Junior. A modified fluorescence *in situ* hybridization protocol for *Plasmodium falciparum* greatly improves nuclear architecture conservation. *Molecular and Biochemical Parasitology*, 173(1):48–52, 2010.

[14] H. Tjong, K. Gong, L. Chen, and F. Alber. Physical tethering and volume exclusion determine higher-order genome organization in budding yeast. *Genome Res*, 22(7):1295–1305, 2012.